Journal of Volcanology and Geothermal Research 303 (2015) 59–78

Contents lists available at ScienceDirect

Journal of Volcanology and Geothermal Research

journal homepage: www.elsevier.com/locate/jvolgeores

Glaciovolcanism at Volcán Sollipulli, southern Chile: Lithofacies analysis and interpretation

Stefan M. Lachowycz [a,*], David M. Pyle [a], Jennie S. Gilbert [b], Tamsin A. Mather [a], Katy Mee [c], José A. Naranjo [d], Laura K. Hobbs [b]

[a] Department of Earth Sciences, University of Oxford, South Parks Road, Oxford OX1 3AN, United Kingdom
[b] Lancaster Environment Centre, Lancaster University, Lancaster LA1 4YQ, United Kingdom
[c] British Geological Survey, Environmental Science Centre, Keyworth, Nottingham NG12 5GG, United Kingdom
[d] Servicio Nacional de Geología y Minería, Avenida Santa María 0104, Santiago, Chile

ARTICLE INFO

Article history:
Received 18 December 2014
Accepted 20 June 2015
Available online 3 July 2015

Keywords:
Volcano–ice interaction
Glaciovolcanic lithofacies
Hyaloclastite
Stratovolcano
Caldera
Paleoenvironment reconstruction

ABSTRACT

Magma–ice–meltwater interactions produce diverse landforms and lithofacies, reflecting the multitude of factors that influence glaciovolcanism, including both magmatic (e.g., composition, eruption rate) and glacial (e.g., ice thickness, thermal regime) conditions. This is exemplified by the walls of the partly ice-filled summit caldera of Volcán Sollipulli, a stratovolcano in southern Chile, which include lithofacies from eruptions of a wide range of magma compositions beneath or in contact with ice. Here we analyse these lithofacies and hence propose new interpretations of the eruptive and glacial history of Sollipulli. The facies include a thick, laterally extensive sequence of fragmental glaciovolcanic deposits, comprising massive, mafic lava pillow-bearing hyaloclastite overlain by sills and then hyaloclastic debris flow deposits (similar to Dalsheidi-type sequences). The distribution and thickness of these units indicate an unusual abundance of magma–meltwater interaction for an arc stratovolcano in temperate latitudes, perhaps due to eruptions beneath a thick ice cap. Coherent lava coulées, domes, lobes, and stacks of basaltic andesite–trachydacite composition are present around the top of the caldera rim; these display morphologies and fracture patterns on caldera-facing margins that indicate that the caldera was filled with ice when these lavas were erupted. The lithofacies characterised in this study demonstrate the diversity of glaciovolcanism that is possible at arc stratovolcanoes capped by temperate ice or with ice-filled calderas, and the potential for uncertainties in inference of the palaeoenvironmental conditions of their emplacement.

1. Introduction

Glaciovolcanism, the interaction between erupting magma and ice (in any form) and the resulting meltwater, is a widespread phenomenon on Earth and Mars (Smellie and Chapman, 2002), the significance of which is increasingly being recognised (Russell et al., 2014). For example, such activity can generate or exacerbate certain volcanic hazards (Tuffen, 2010), such as lahars and floods (e.g., Major and Newhall, 1989), edifice collapse (e.g., Huggel, 2009), and secondary phreatomagmatic explosions (e.g., Belousov et al., 2011). The responses of these hazards and rates of volcanism to past glacial cycles and future climate change are poorly constrained (Tuffen, 2010; Watt et al., 2013). Furthermore, volcano–ice interactions create a distinctive and wide-ranging suite of landforms (e.g., Smellie, 2009, 2013; Russell et al., 2014) and lithofacies (e.g., Smellie et al., 1993; Loughlin, 2002; Skilling, 2009), which are an invaluable source of terrestrial palaeoenvironmental information (e.g., palaeoice distribution, thickness, and thermal regime: e.g., Smellie, 2009; Tuffen et al., 2010; Smellie et al., 2014), especially prior to the last glaciation (e.g., McGarvie et al., 2007; Smellie et al., 2011, 2014) and on Mars (e.g., Smellie, 2009). Detailed characterisation of the products of glaciovolcanism in each particular setting is necessary to understand their formation processes and the associated hazards, as well as their palaeoenvironmental significance.

Volcano–ice interactions have been studied most extensively in Antarctica, Iceland, and western North America. Tuyas (as defined by Russell et al., 2014), lava-fed deltas (e.g., Skilling, 2002; Smellie et al., 2013, 2014), and sheet-like sequences (e.g., Smellie et al., 1993; Smellie, 2008) are the most common glaciovolcanic landforms in these regions (Smellie, 2009, 2013), except parts of western North America (e.g., Lescinsky and Fink, 2000; Kelman et al., 2002). Glaciovolcanism at stratovolcanoes in continental arcs and/or at temperate latitudes may be distinct, as coherent lavas with fracture patterns

* Corresponding author at: Department of Earth Sciences, University of Oxford, South Parks Road, Oxford, Oxfordshire OX1 3AN, United Kingdom. Tel.: +44 1865 272000.
E-mail addresses: stefan.lachowycz@earth.ox.ac.uk (S.M. Lachowycz), david.pyle@earth.ox.ac.uk (D.M. Pyle), j.s.gilbert@lancaster.ac.uk (J.S. Gilbert), tamsin.mather@earth.ox.ac.uk (T.A. Mather), katy@bgs.ac.uk (K. Mee), jose.naranjo@sernageomin.cl (J.A. Naranjo), l.hobbs@lancaster.ac.uk (L.K. Hobbs).

http://dx.doi.org/10.1016/j.jvolgeores.2015.06.021
0377-0273/

and/or morphologies indicative of contact with and confinement by ice (e.g., Lescinsky and Fink, 2000) appear to be more typical than these landforms and fragmental glaciovolcanic lithofacies. This has been reported to be the case at volcanoes including Hoodoo Mountain (Edwards and Russell, 2002) and some in the Garibaldi Volcanic Belt (Kelman et al., 2002) in British Columbia, Nevados de Chillán in Chile (Mee et al., 2006, 2009), Ruapehu in New Zealand (Spörli and Rowland, 2006; Conway et al., 2015), and the United States Cascades (e.g., Lescinsky and Sisson, 1998; Lescinsky and Fink, 2000), although hyaloclastite is noted locally at some volcanoes (e.g., Mee et al., 2009; Schmidt and Grunder, 2009). This difference has been attributed to the comparative rarity of considerable interaction with meltwater (e.g., producing pillow lava or hyaloclastic or phreatomagmatic breccia/tuff: e.g., Loughlin, 2002) in the latter case (Lescinsky and Fink, 2000; Kelman et al., 2002). This was suggested to reflect felsic magmas and alpine-type glacial regimes generally being common at such volcanoes (e.g., in the Andes: Stern, 2004; Rabassa, 2008; Rivera and Bown, 2013): more silicic magmas melt relatively little ice, and meltwater can drain more readily from beneath alpine-type glaciers than ice caps or sheets (Höskuldsson and Sparks, 1997; Kelman et al., 2002); meltwater retention is more likely to be the limiting factor (Stevenson et al., 2009). Nevertheless, it is unclear whether this is a genuine difference between Antarctic or Icelandic and most continental arc glaciovolcanism, or simply a reflection of the relatively few studies of the latter.

In this study, we analyse and interpret glaciovolcanic lithofacies observed on Volcán Sollipulli, a glaciated (i.e., previously glacierised) stratovolcano in southern Chile with a summit caldera that is currently partially filled with ice. In contrast to most of the few previous studies of glaciovolcanism at arc stratovolcanoes, the eruption products described result from diverse magma compositions, and include both an extensively distributed variety of fragmental glaciovolcanic lithofacies and examples of interaction between lava and intra-caldera ice.

2. Volcán Sollipulli

2.1. Geological and glaciological context

Sollipulli lies in the central sector of the Andean Southern Volcanic Zone (SVZ) of Chile and Argentina (at 38.97°S, 71.52°W), ~25 km east of the volcanic front between Llaima and Villarrica volcanoes (Fig. 1). The geological setting of volcanism and the history of explosive eruptions in this region have been reviewed by Stern (2004) and Fontijn et al. (2014) respectively. Of the 74 volcanic centres in southern Chile and Argentina that are thought to have been active since the last glacial period (Fontijn et al., 2014), Sollipulli is one of the 43 that are at least partly ice-covered at present, and one of the (at least) 20 volcanoes known or suspected to have an ice-filled summit crater or caldera (Siebert et al., 2010; Rivera and Bown, 2013) (Fig. 1; listed in Supplementary File 1). The ~4 km wide caldera at Sollipulli (Fig. 2) contained an estimated 4.5 ± 0.5 km^3 of ice to a maximum depth of 593 ± 59 m in February 2011 (Hobbs, 2014), which has reduced in extent and depth over at least the last 50 years (Rivera and Bown, 2013; Hobbs, 2014). Permanent ice is currently almost absent from the flanks of the volcano (Fig. 2), but there is seasonal snow cover. The volcanoes of

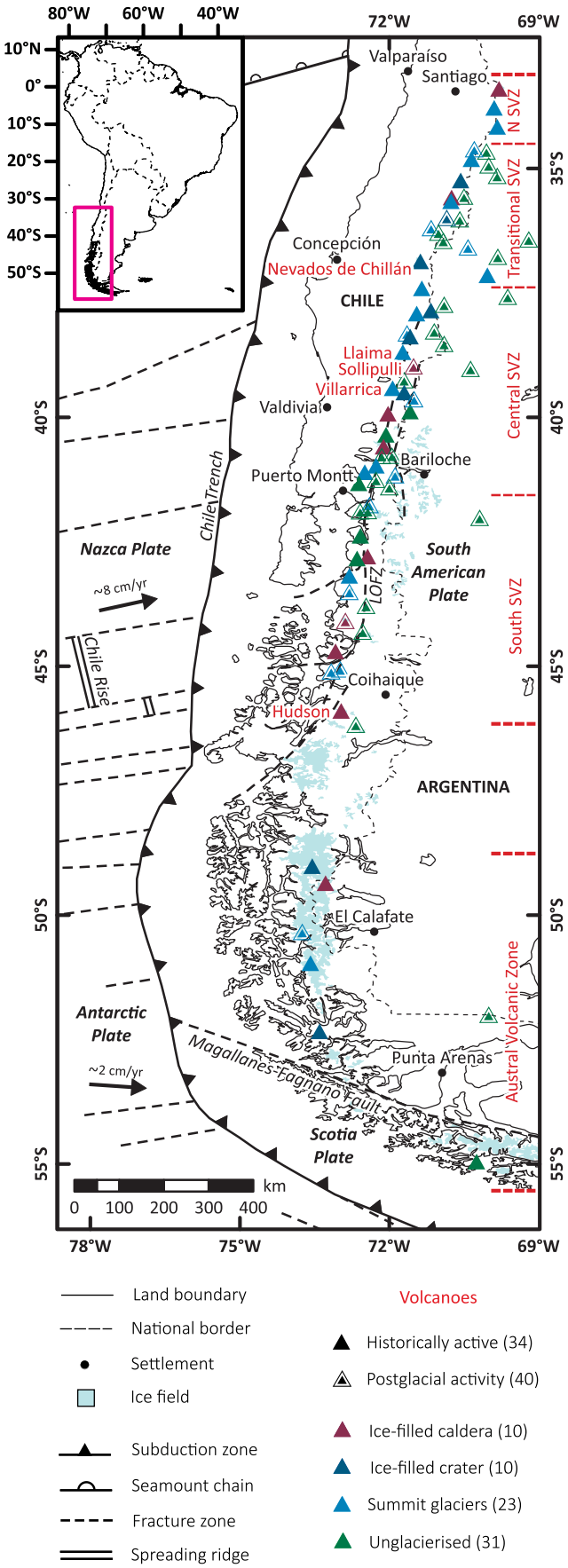

Fig. 1. Map of southern Chile showing the volcanic centres of the Andean Southern Volcanic Zone (SVZ) and Austral Volcanic Zone (AVZ) for which there is evidence of activity since local glacial retreat (listed in Supplementary File 1; modified from Fontijn et al., 2014). The volcanoes are classified by the timing of their most recent known eruption and the presence of glaciers or an ice-filled crater (≤1 km diameter) or caldera (>1 km) (Siebert et al., 2010; Rivera and Bown, 2013); the abundance of glacierised volcanoes shows the considerable potential for glaciovolcanism in this region (Section 2.1). The labelled volcanoes are referred to in this paper. Some regional tectonic features that are potentially a significant control on the location of volcanism are also delineated (Bird, 2003; Stern, 2004; Matthews et al., 2011), e.g. the Liquiñe-Ofqui Fault Zone (LOFZ; López-Escobar et al., 1995). The geographical data are from Natural Earth (naturalearthdata.com).

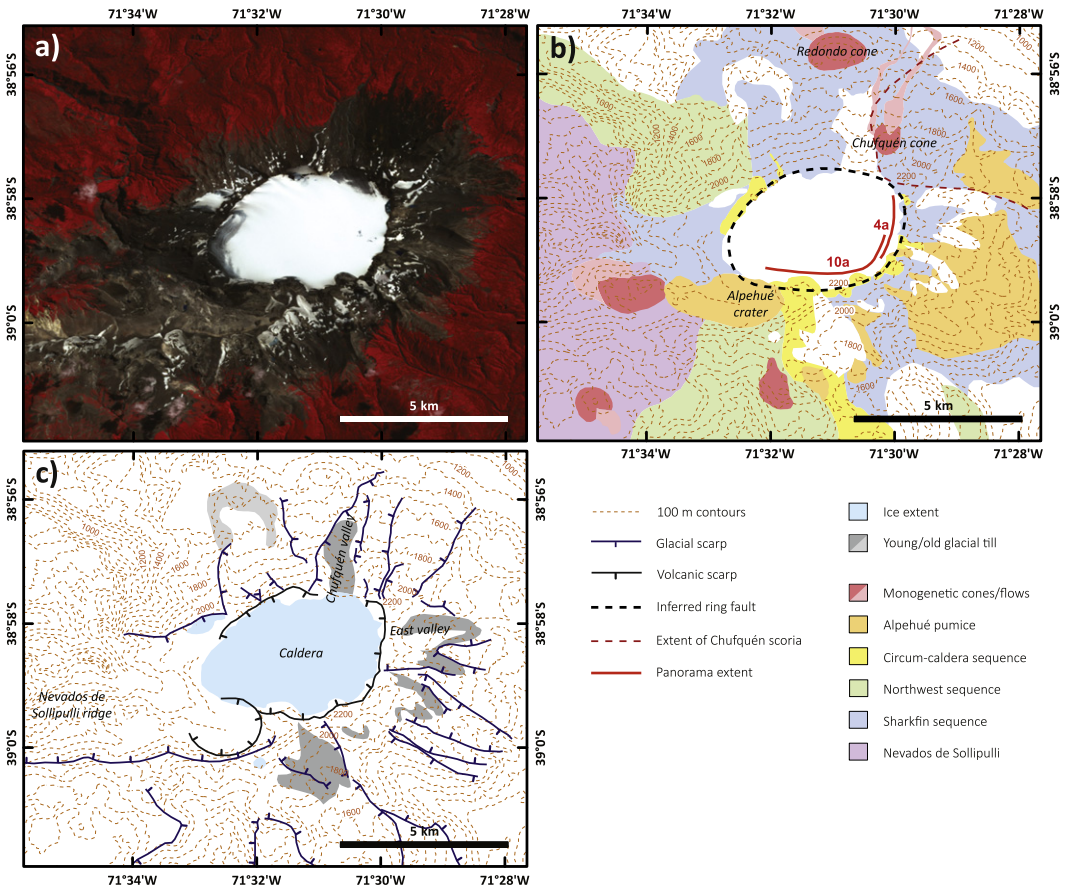

Fig. 2. (a) Orthorectified ASTER false colour (RGB321) image (USGS and Japan ASTER program, 2012) taken in February 2005, which shows the upper flanks and summit caldera of Volcán Sollipulli. Note the ice-filled caldera and the scarcity of snow cover on the flanks (Section 2.1). (b) A topographic map of the same area, overlain by our interpretation of the geology, updated from those presented by previous studies (Naranjo et al., 1993a; Gilbert et al., 1996; Murphy, 1996) (Section 2.2); the mapped units are summarised in Table 1. The geology away from the caldera rim is largely poorly constrained. The red lines indicate the sectors of the caldera wall shown in Figs. 4a and 10a. (c) A map of the topography and selected geomorphological features in the same area. The ice extent in the satellite image is mapped, along with glacial scarps and till deposits, from satellite and aerial imagery; the latter constrain the extent and timing of past glaciation in the summit region (Section 2.3). Some of the labelled locations are referred to in the text.

the southern Andes were covered by ice at the Last Glacial Maximum (LGM, ~26.5–18 ka here) (Glasser et al., 2008; Clark et al., 2009; Watt et al., 2013); the extent and timing of prior glacierisations are poorly constrained (Rabassa, 2008), despite the importance of understanding glacial variations in southern South America for palaeoclimatology (e.g., Hulton et al., 2002; Glasser et al., 2008). Glaciovolcanism could provide significant data on past glaciation, yet there are few published studies of volcano–ice interaction in this region (Gilbert et al., 1996; Mee et al., 2006, 2009).

2.2. Eruptive history

Sollipulli has erupted a wide range of magma compositions, from basalt to trachydacite (Fig. 3). The oldest volcanic rocks on Sollipulli are thought to be Pleistocene in age, and erupted due to migration of volcanism away from the Nevados de Sollipulli complex, which forms a ridge to the west of Volcán Sollipulli (Fig. 2) (Naranjo et al., 1993a). The age of the caldera has not previously been constrained; no major pyroclastic units have been attributed to Sollipulli other than those of the post-caldera Alpehué Plinian eruption (Naranjo et al., 1993a; Fontijn et al., 2014), so the caldera is thought to have formed by a non-explosive mechanism (Gilbert et al., 1996). The main eruptive sequences that have been identified are summarised in Table 1, which includes new Ar–Ar and modelled radiocarbon dates for units in some of these sequences; supporting data for these are provided in Supplementary

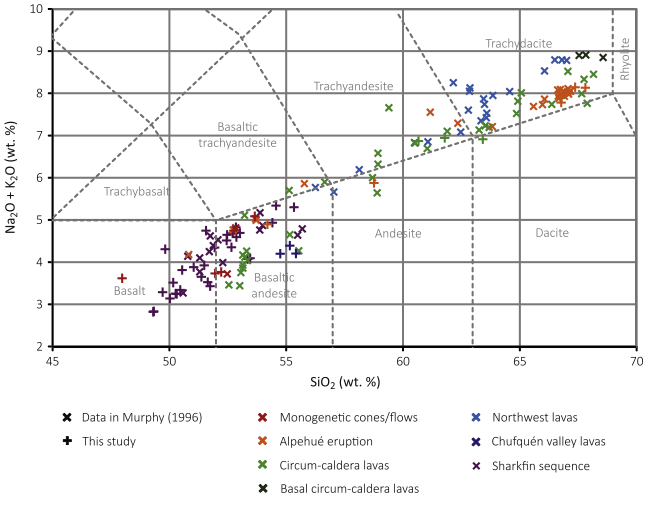

Fig. 3. Total alkali–silica plot (Le Bas et al., 1985) of the whole rock composition of specimens from some of the sequences/units listed in Table 1 and described in Section 3. All the data are component oxide weight percentages measured by X-ray fluorescence, recalculated to consider loss on ignition (except when this is negative). The new data presented are for samples prepared using the method of Ramsey et al. (1995) and analysed at the Department of Geology, University of Leicester. Note the clear trends within and mostly distinct nature of the composition of the majority of the sequences/units.

Table 1
Summary of the main parts of the stratigraphy of the upper flanks of Sollipulli, modified from Gilbert et al. (1996) to incorporate data from Naranjo et al. (1993a), Murphy (1996), De Vleeschouwer (2002), Fontijn et al. (in preparation), Jara and Moreno (in preparation), and this study.

Sequence/unit	Age constraints		Composition[g]	Description	Interpretation
	Stratigraphy	Radiometric dating			
Chufquén	Overlies all other units.	633 ± 87 cal yr BP[a,b]	Basaltic andesite	Scoria cones on the upper NE flank, with a ~6.5 km long ʻaʻā lava; scoria fall across NE flank.	Subaerial eruption; monogenetic.
Alpehué	Post-CFE: tephra overlies circum-caldera lava sequence.	2938 ± 110 cal yr BP[a,c]	Trachydacite mixed with basaltic andesite	Pumice-rich tephra fall to the north and east of caldera, pyroclastic density current deposits to the south and NW, and lahar deposits to NW.	Plinian eruption.
Redondo	Pre-Alpehué: Alpehué tephra found on summit of scoria cone.		Basalt	Scoria cone on the north flank, with a ~3.5 km long ʻaʻā lava.	Subaerial eruption; monogenetic.
Circum-caldera (Section 3.4)	Post-CFE: vents are located on the caldera rim; evidence for interaction with intra-caldera ice.	26 ± 5 ka[d], 64 ± 15 ka[f], 68 ± 14 ka[d]	Basaltic andesite to trachydacite	Fractured lava domes, coulées, lobes, and sheets on the caldera rim, often overlain by thin ʻaʻā lavas.	Lavas extruded from a ring dyke, and either constrained by ice or erupted subaerially above the ice level.
Chufquén valley (Section 3.3)	Post-date the erosion of the Chufquén valley, so considerable time after the Sharkfin sequence.		Basaltic andesite	Fractured or marginally brecciated lavas in the upper Chufquén valley.	Subaerial, flooded, and ice-constrained effusive eruptions.
Northwest	Overlain by the circum-caldera lavas. Appears to overlie the Sharkfin sequence. Prior to CFE?	100 ± 30 ka[e], 110 ± 30 ka[e], 120 ± 14 ka[f], 120 ± 16 ka[f]	Dacite (and andesite?) with mafic inclusions	Thin ʻaʻā lavas, with a few fractured lavas from a later flank eruption. The top of the sequence has glacial striae.	Subaerial effusive eruptions. Glacial advance after lava emplacement.
Sharkfin (Section 3.2)	Pre-CFE: forms part of the caldera walls. Overlain by the circum-caldera lava sequence.	350 ± 90 ka[d], 700 ± 140 ka[d]	Basalt to basaltic andesite	Thin ʻaʻā lavas, pillow lava and palagonitised tuff-breccias, and palagonitised debris flow deposits with scoria units; abundant intrusions.	Predominantly subglacial/subaqueous eruptions.
Other scoria cones	Unconstrained		Basalt to basaltic andesite?	Other scoria cones, some with lavas.	Eruptions similar to the Chufquén and Redondo cone-forming events.
Nevados de Sollipulli	Assumed Pliocene/Pleistocene.	312 ± 20 ka[e], 490 ± 30 ka[f]	Basaltic andesite to dacite?	Composite ridge of multiple sequences of lavas and tuff-breccias, possibly including hyaloclastite.	Various subaerial and/or subglacial eruptions.

CFE = caldera-forming event.
[a] ^{14}C dates calibrated in OxCal v4.2.4 (Bronk Ramsey, 2009) using the SHCal13 atmospheric calibration curve (Hogg et al., 2013); 2σ confidence interval.
[b] Single date from Naranjo et al. (1993a) (Supplementary File 3).
[c] Date for eruption from Bayesian modelling (in OxCal v4.2.4) incorporating multiple dates and stratigraphic constraints (Supplementary File 3).
[d] Plateau Ar–Ar dates obtained from groundmass samples for this study (Supplementary File 2); 2σ confidence interval.
[e] Plateau and [f] isochron Ar–Ar dates from groundmass samples to be published in Jara and Moreno (in preparation); 2σ confidence interval.
[g] The whole-rock composition ranges of most of these sequences/units are shown in Fig. 3.

Files 2 and 3. The approximate distributions of some of the main sequences, inferred from aerial and satellite imagery with limited ground-truthing, are shown in Fig. 2b.

Earlier work on Sollipulli (Gilbert et al., 1996; Murphy, 1996) noted evidence of glaciovolcanism, and deduced changes in ice thickness through the eruptive history. However, the stratigraphy we examine here has not previously been described and interpreted in detail. We focus on the lava and fragmental lithofacies units that are exposed on the walls of the east to south sectors of the caldera and in the uppermost Chufquén valley (Fig. 2), which mostly comprise the 'Sharkfin', 'South', and 'Peak' units described by Gilbert et al. (1996). The pre-caldera Sharkfin sequence was previously interpreted as deposits from subglacial or subaqueous eruptions that became subaerial. The South and (overlying) Peak units, hereafter grouped as the 'circum-caldera' lava sequence (similar to Murphy (1996)), were respectively interpreted as ice-constrained and subaerial lavas emplaced on the margin of the caldera after it had formed (Gilbert et al., 1996).

2.3. Geomorphological constraints on glacial history

From aerial and satellite imagery, we map several till deposits and numerous scarps on the upper flanks of Sollipulli (Fig. 2c). With the exception of those forming the walls of the caldera and the Alpehué crater, the scarps are roughly slope-parallel (i.e., mostly radiate from the caldera); we infer that these originate from glaciation. With further geological mapping and radiometric dating, the relationships between these features and the geology with which they are associated could constrain the timing and extent of glaciation of the volcano, to complement inferences from the evidence of glaciovolcanism. For example, most of the young till deposits mapped in Fig. 2c appear to overlie pumice deposits from the Alpehué eruption, and possibly also scoria from the Chufquén eruption in the Chufquén and East valleys (Figs. 2b and 2c). This suggests that these till deposits mark the maximum extent of glaciers in the past ~2.9 kyr, or possibly the past ~630 yr, considering the dates of those eruptions (Table 1). The Chufquén and East valleys themselves have eroded through the Sharkfin sequence, so must post-date its emplacement < ~350 kyr ago (Table 1), and the Chufquén valley must pre-date the eruption of the (undated) Chufquén valley lavas.

3. Lithofacies and sequence descriptions

3.1. Lithofacies classification

We recognise 16 discrete volcanic lithofacies in the eruptive sequences described in this article; a summary description and interpretation and the assigned code for each lithofacies are listed in Table 2. No glaciogenic deposits were identified within the sequences studied. The grain size and classification terms used are as defined for primary

volcaniclastic rocks by White and Houghton (2006). Discrete classification of the lithofacies in the Sharkfin sequence (Section 3.2) is challenging due to their diversity and complex associations, typical of some glaciovolcanic sequences (e.g., Smellie et al., 1993; Loughlin, 2002; Skilling, 2002). We distinguish lava, tuff-breccia, lapilli-tuff, and tuff; lavas are differentiated by morphology, and fragmental deposits by their componentry and then sorting, association, or composition. Some of the lithofacies accompany one another (e.g., coherent lava with lava margin tuff-breccia), but not exclusively, so they are not grouped together. Some additional subdivisions were rejected because the resulting lithofacies would be distinguished only by characteristics that are not always present (e.g., bedforms) or can be ambiguous (e.g., stratigraphic context).

This classification scheme is similar to those of (for example) Loughlin (2002), Skilling (2009), and Watton et al. (2013). In contrast to those studies, we do not use hyaloclastite as a lithofacies descriptor (despite many of the palagonite-bearing lithofacies being interpreted as hyaloclastic), due to its genetic connotations. The term hyaloclastite has previously been ascribed to a variety of volcaniclastic rock types formed both by primary fragmentation and reworking, as outlined by Watton et al. (2013). Here it is used as prescribed by Rittman (1958), for deposits that are thought to result from predominantly passive (quench and mechanical) magma fragmentation, with only relatively limited explosive lava–water interaction (e.g., Skilling, 2009; Watton et al., 2013), but also including those locally remobilised (Watton et al., 2013). However, some studies have argued or assumed that (phreato)magmatic fragmentation is the dominant process forming such rocks (e.g., Tuffen, 2007; Edwards and Russell, 2011; Pollock et al., 2014).

3.2. Sharkfin sequence

We subdivide the Sharkfin sequence into three main subsequences, described below; the stratigraphy (including that of the circum-caldera lavas where overlying this sequence) in the areas studied is summarised in Fig. 4.

3.2.1. Sharkfin lava subsequence

This subsequence is principally present at the bottom of the Sharkfin sequence in the SE sector of the caldera wall (Fig. 4a), but is occasionally also above the hyaloclastite subsequence (Fig. 4d). It predominantly comprises porphyritic basaltic ‘a’ā lavas of varying vesicularity and (plagioclase, olivine, and minor clinopyroxene) phenocryst content; a representative exposure is presented in Fig. 5. The coherent lava units, usually cut into sub-metre-sized blocks by irregular fractures, range in thickness from ~0.3–1.5 m, and are bounded by tuff-breccia units of a similar thickness range (Fig. 5a). This tuff-breccia, which is generally clast-supported, is composed of poorly sorted, often scoriaceous lapilli- to block-sized angular lava fragments in a typically uniform, oxidised matrix, which comprises ash- to fine lapilli-sized glass and crystal fragments (Fig. 5b). The majority of the finest-grained component of this matrix is palagonitised glass, which is uniformly distributed within the breccia. Some of the lava-breccia packages are separated by a <0.5 m thick layer of well-sorted medium ash- to fine lapilli-sized palagonitised glass and crystal fragments. These layers infill cavities in underlying units and appear to have been altered/oxidised where in proximity to and partly mixed with the overlying lava margin deposits (Figs. 5b and 5c). This overlying unit of lapilli-tuff has a higher proportion of smaller clasts and a lower clast:matrix ratio than the tuff-breccia elsewhere in the subsequence (Fig. 5b).

The top of this subsequence is delineated by the first occurrence of massive palagonitised tuff-breccia or lapilli-tuff (hyaloclastite subsequence: Section 3.2.2), which sometimes cross-cuts the uppermost lavas (Fig. 4d). There is no evidence of grading or apophyses of the lava into the hyaloclastite, which are often present in Mt Pinafore-type (sheet-like) sequences (Smellie et al., 1993; Smellie and Skilling, 1994). The base of the subsequence is not exposed; the largest exposure of these lavas is at least ~11 m thick (Fig. 4g). All but the thinnest units appear to be laterally continuous in the caldera wall for at least several metres (e.g., Fig. 4e), but it is not possible to confidently correlate individual units between the main outcrops. The downslope continuation of the subsequence was not confirmed due to the inaccessibility of the slopes. The main outcrops in the caldera walls were not described by Gilbert et al. (1996) because they have been exposed by the intra-caldera ice retreat since this earlier study (Hobbs, 2014).

3.2.2. Sharkfin hyaloclastite subsequence

This subsequence mostly comprises pillow lava and massive tuff-breccia containing poorly sorted, lapilli- to block-sized monomict angular lava clasts (some discernible as pillow fragments) in a palagonitised matrix. This matrix is composed of medium ash- to fine lapilli-sized palagonitised glass and crystal fragments; matrix-dominated (i.e., palagonitised lapilli-tuff and tuff) lithofacies are present, but relatively uncommon. Example outcrops are shown in Fig. 6. The lava components are of basalt to basaltic andesite composition, with occasional plagioclase, olivine, and minor clinopyroxene phenocrysts and, notably, variable vesicularity (from 0% to ~60%; e.g., compare Fig. 6b and Fig. 6f). There is considerable spatial variation (usually gradational) in pillow form (e.g., shape, fracturing, and fragmentation extent) and size, and clast size distribution and clast:matrix ratio, but no consistent stratigraphy (e.g., Fig. 6a). The lithofacies present form a continuum from fractured irregular lava pillows (up to ~1 m tall and a few metres long; e.g., Fig. 6b) through increasingly disaggregated lava masses (e.g., Fig. 6c) to angular to subrounded lava fragments (e.g., Fig. 6d), in an increasing proportion of matrix. Where they appear to be in situ, the lava pillows have highly fragmented margins, for example surrounded by tuff-breccia that is increasingly rich in palagonitised matrix away from the pillow centre (Fig. 6b) or by fragments of chilled margin (Fig. 6f), irrespective of the vesicularity of the lava. In places, pillows are isolated in tuff-breccia (i.e., matrix supported); a range of pillow:breccia ratios are observed (e.g., compare Fig. 6c and Fig. 6e). Pillow-bearing or clast-rich tuff-breccia can occasionally be found as lenses or sheets within palagonitised lapilli-tuff/tuff sorted to varying extents (Fig. 6g). The frequent gradational spatial variations in lithofacies mean that it is not possible to correlate units within this subsequence between outcrops.

Most of the studied outcrops of this subsequence are cut by dykes, the majority of which are <2 m in width and similar in composition to the lava pillows and clasts in the tuff-breccia or lapilli-tuff. Some of these dykes appear to feed lava pillows or upper parts of the subsequence (e.g., Fig. 4d), and some are truncated at the contact with the overlying debris flow subsequence (e.g., Fig. 6g). Groundmass samples from two of these truncated dykes (marked on Fig. 4) have been Ar–Ar dated by the method outlined in Arancibia et al. (2006) to 350 ± 90 and 700 ± 140 ka (Supplementary File 2). The former of these coincides with a cool marine isotope stage during a glacial period (MIS 10, ~374–337 ka; Lisiecki and Raymo, 2005); the latter has a mean square weighted deviation (MSWD) ≪ 1 (Supplementary File 2), so is unlikely to be robust. Therefore, the difference between the two dates does not necessarily indicate a long hiatus between the emplacement of the hyaloclastite and debris flow subsequences. The base of the debris flow subsequence clearly cuts into underlying units in places (e.g., Fig. 4b), indicating erosion of parts of the hyaloclastite subsequence, which may account for its variable thickness, from ~2 to >12 m (Fig. 4g). Outcrops of this subsequence are recognised in all sectors of the caldera wall where the Sharkfin sequence is exposed (Figs. 2 and 4), rather than just some parts as reported by Gilbert et al. (1996); the additional outcrops have been exposed by the intra-caldera ice retreat since this earlier study (Hobbs, 2014). Lithofacies found in this subsequence have also been recognised on the uppermost flanks that were accessible, on the north, northeast (including at one location ~1.5 km down the Chufquén valley (Gilbert et al., 1996)), and east sides.

Table 2
Summary descriptions and interpretations of the discrete volcanic lithofacies identified in the outcrops studied on Sollipulli.

Lithofacies		Code	Occurrence	Examples	Description	Common associations	Interpretation
Lavas	Coherent lava	*Lc*	CC, CV, SL	Fig. 5 Fig. 9c	Lava with only a low density of irregular blocky or columnar fractures, occasionally with reddened surfaces. ~0.5 to tens of metres thick. Commonly grades into or is bounded by tuff-breccia or fractured lava with lava fragments of the same composition.	*BCl*, *Lf*	(Interior of) lavas emplaced subaerially or with minimal interaction with ice or water (e.g., beneath snow or a freely draining thin glacier).
	Highly fractured lava	*Lf*	CC, CV	Fig. 9a Fig. 10b	Lava that is pervasively fractured, typically in patterns indicative of rapid cooling (e.g., hackly), with negligible palagonite--bearing tuff or tuff-breccia. Present towards margins of ~1 to tens of metres thick coulées, domes, lobes, and sheets.	*Lc*, *BCl*	Lava cooled rapidly by meltwater saturation/penetration resulting from contact with ice. The orientation, distribution, and pattern of fracturing reflect the nature of the cooling front.
	Pillow lava (with minor tuff-breccia)	*Lp*	SH	Fig. 6b	Mostly intact lava pillows ~0.3 to a few metres across, often elongate or irregular in shape, irregularly or radially fractured, and/or brecciated at their margins. <30% interstitial palagonitised fine-grained matrix with lapilli–block-sized angular lava fragments.	*BC*, *BMp*, *BM*	Lava erupted into ponded meltwater beneath ice, with only marginal quench fragmentation forming interstitial hyaloclastic tuff-breccia.
Clast-supported tuff-breccias	Clast-supported tuff-breccia	*BC*	SH	Fig. 6b Fig. 6g	Predominantly clast-supported tuff-breccia comprising poorly sorted, lapilli–block-sized angular lava fragments in a matrix of ash–fine lapilli-sized palagonitised glass and crystal fragments. Bedding rare. Can grade into and/or contain pods of matrix-supported tuff-breccia.	*Lp*, *BMp*, *BM*	Subaqueous lava (erupted into ponded meltwater beneath ice), brecciated by passive quench and mechanical fragmentation.
	Lava margin tuff-breccia	*BCl*	CC, CV	Fig. 9c Fig. 10g	Predominantly clast-supported tuff-breccia comprising poorly sorted, lapilli–block-sized angular lava fragments in a (sometimes oxidised) matrix of ash–fine lapilli-size fragments. Often bounds coherent lava.	*Lc*, *Lf*	Marginal autobreccia of subaerial 'aʻā or blocky lava.
	Lava margin palagonite-bearing tuff-breccia	*BClp*	SL	Fig. 5	Predominantly clast-supported tuff-breccia comprising poorly sorted, lapilli–block-sized angular lava fragments in a slightly oxidised matrix of ash–fine lapilli-sized fragments of crystals and partially palagonitised glass. Bounds some coherent lava units.	*Lc*	Marginal autobreccia of lavas, with some palagonitised glass from quench fragmentation and alteration due to the presence of meltwater during emplacement (beneath ice?).
Matrix-supported tuff-breccias	Matrix-supported tuff-breccia	*BM*	SD, SH	Fig. 6a Fig. 7b	Predominantly matrix-supported tuff-breccia comprising poorly-sorted, predominantly block-sized, usually angular lava fragments in a matrix of ash–fine lapilli-sized palagonitised glass and crystal fragments. Bedding rare; can form lenticular units.	*BC*, *BMp*, *TL*, *Tp*	From fragmentation of lava erupted into ponded meltwater beneath ice; sometimes remobilised by slumping and/or meltwater flow.
	Pillow lava-bearing tuff-breccia	*BMp*	SH	Fig. 6c Fig. 6e	Predominantly matrix-supported tuff-breccia comprising isolated (typically irregular) lava pillows and/or pillow fragments, together with poorly sorted, predominantly block-sized angular lava fragments in a matrix of ash–fine lapilli-sized palagonitised glass and crystal fragments. Bedding rare.	*Lp*, *BC*, *BM*	Sliding or emplacement of pillows into more fragmented primary or remobilised deposits, and/or brecciated by enhanced mechanical or quench fragmentation. Subaqueous (erupted into ponded meltwater beneath ice).
	Oxidised scoria-bearing tuff-breccia	*BMs*	SD	Fig. 7e	Poorly sorted, lapilli–block-sized angular scoria clasts/fragments with oxidised surfaces in a red oxidised matrix of ash–fine lapilli-sized fragments of scoria, crystals, and palagonitised glass. Clast:matrix ratio highly variable. Occasional planar bedding.	*TLp*, *TLw*, *Tb*, *Tp*	Subaerial spatter/explosive eruption deposits reworked in debris flows.
Lapilli-tuffs	Lapilli-tuff	*TL*	SD, SH	Fig. 6d	Predominantly matrix-supported lapilli-tuff comprising generally lapilli-sized, mostly angular lava fragments in a matrix of ash–fine lapilli-sized palagonitised glass and crystal fragments; variable sorting. Bedding only when associated with bedded units.	*BMp*, *BM*, *TLp*	Relatively fine-grained fraction of deposits from fragmentation of lava erupted into ponded meltwater beneath ice; likely remobilised by meltwater flow.
	Lava margin palagonite-bearing lapilli-tuff	*TLlp*	SL	Fig. 5	Predominantly matrix-supported lapilli-tuff comprising poorly sorted, lapilli-sized angular lava fragments in a slightly oxidised matrix of ash–fine lapilli-sized fragments of crystals and partially palagonitised glass. Grades into altered palagonite-rich tuff.	*Lc*, *TLpa*	Basal lapilli-tuff of lavas emplaced on a palagonite-rich sediment layer.
	Poorly sorted palagonite-rich lapilli-tuff	*TLp*	SD, SH	Fig. 6g Fig. 7d	Matrix-supported lapilli-tuff comprising <30% poorly sorted, typically lapilli-sized subangular lava fragments, in a matrix of ash–fine lapilli-sized palagonitised glass and crystal fragments. Massive or (less commonly) planar-bedded units.	*TLw*, *Tp*	Subglacial eruption deposits reworked in relatively high-energy debris flows (due to subglacial meltwater drainage).

Table 2 (*continued*)

Lithofacies		Code	Occurrence	Examples	Description	Common associations	Interpretation
	Well-sorted palagonite-rich lapilli-tuff	*TLw*	SD, SH	Fig. 6g Fig. 7d	Matrix-supported lapilli-tuff comprising <30% well-sorted, typically lapilli-sized subangular lava fragments in a matrix of ash–fine lapilli-sized palagonitised glass and crystal fragments. Massive, or planar-bedded units that sometimes extend >100 m downslope.	*TLp*, *Tp*	Finer-grained fractions of subglacial eruption deposits reworked in relatively low-energy debris flows (due to subglacial meltwater drainage); extensive deposits from outburst floods.
Tuffs	Palagonite-rich tuff	*Tp*	SD, SH, SL	Fig. 5 Fig. 7b	Well-sorted ash–fine lapilli-sized fragments of palagonitised glass and crystals, with rare lava fragment clasts. Sometimes infills cavities in underlying units; can also form massive or (usually) planar-bedded units that sometimes extend >100 m downslope.	*TLp*, *TLw*, *TLlp*, *BClp*	Fine-grained matrix fraction of subglacial eruption deposits reworked in relatively low-energy debris flows (due to subglacial meltwater drainage); extensive deposits from outburst floods.
	Altered palagonite-rich tuff	*Tpa*	SL	Fig. 5	Well-sorted medium tuff–fine lapilli-tuff comprising fragments of palagonitised glass and crystals, increasingly altered and with increasingly abundant lapilli–block-sized lava clasts towards contacts with overlying lava margin palagonite-bearing tuff-breccia.	*Tp*, *TLlp*	Redeposited fine-grained matrix fraction of subglacial eruption deposits, which have been thermally altered and partially mixed with the basal lapilli-tuff of a lava flow emplaced on top.
	Bedded tuff	*Tb*	SD	Fig. 7e	Finely planar bedded/laminated (or occasionally massive), very well-sorted ash–lapilli-sized tephra. Variable palagonitisation and lithification.	*Tp*, *BMs*	Explosive subaqueous (phreatomagmatic)? eruption deposits. Potentially reworked.

CC = Circum-caldera lava sequence; CV = Chufquén valley lavas; SD = Sharkfin debris flow subsequence; SH = Sharkfin hyaloclastite subsequence; SL = Sharkfin lava subsequence.

3.2.3. Sharkfin debris flow subsequence

This subsequence primarily contains massive and planar- or cross-bedded tuff and lapilli-tuff units, comprising lava clasts in a matrix of medium ash- to fine lapilli-sized palagonitised glass and crystal fragments. Examples of the lithofacies and their relationships are shown in Fig. 7. Both monomict and polymict lapilli-tuff and tuff-breccias are present (e.g., Fig. 7b); the majority of clasts are fine to coarse lapilli-sized, angular to subrounded lava fragments of similar composition to those in the hyaloclastite subsequence. The clast:matrix ratio and extent of sorting are variable (e.g., Figs. 7b and 7d); some units have inversely graded bases and/or irregular elutriation pipes (containing a higher concentration of clasts) (Gilbert et al., 1996). The matrix-supported tuff-breccias sometimes present at the base of the subsequence are distinguishable from the tuff-breccia of the hyaloclastite subsequence by their occurrence as discrete units with contrasting clast sizes and sorting (Fig. 7b). Finely bedded, variably palagonitised/lithified, and well-sorted ash/tuff and lapilli/lapilli tuff units, which sometimes contain lenses of tuff-breccia lithofacies, are observed in some outcrops towards the middle of the subsequence (Fig. 7e). Note that ash-lapilli units do not form the upper units of the subsequence, as thought by Gilbert et al. (1996), which are in fact palagonitised tuff/lapilli-tuff (Figs. 7c and 7d).

Two (or occasionally more) distinctive scoria-bearing units, of highly variable thickness up to ~1.5 m, are present close together in the lower to middle part of this subsequence in most outcrops (see parts of Figs. 4, 7, and 8). These comprise a variable proportion of lapilli- to block-sized oxidised scoria clasts in a matrix that is typically similar in texture to the surrounding units, but with an oxidised component. A dissected scoria cone is present in the NNE caldera wall at approximately the same stratigraphic level as the adjacent debris flow subsequence deposits, but these scoria-bearing units cannot be confidently attributed to this; other possible source scoria cones are present on the upper flanks (Fig. 2b). These units are significant as marker horizons to correlate outcrops of this subsequence. Some other individual units are traceable for tens of metres, both in the caldera rim outcrops and downslope (e.g., Figs. 7a and 7c); these sheet deposits are interspersed with some less extensive units, apparently either eroded (e.g., Fig. 7a) or channelised (e.g., Fig. 7b). Another distinguishing feature of this subsequence is the evidence of soft-sediment deformation on a range of length scales, exemplified in Figs. 7c and 7e.

This subsequence is present in all sectors of the caldera wall where the Sharkfin sequence is exposed; defining the top as the last occurrence of palagonitised deposits, it is up to ~40 m thick (Fig. 4g). The only substantial sills in the Sharkfin sequence are usually present along or just above the contact between this subsequence and the underlying hyaloclastite subsequence. In the caldera wall these sills, which are typically pervasively fractured (but not in a distinctive pattern), form a mostly <2 m thick discontinuous unit along this interface, with an alteration zone <1 m thick only in the underlying hyaloclastite subsequence (e.g., Figs. 4b and 4d). In these outcrops there is no clear evidence of the sills having intruded the overlying debris flow subsequence (e.g., alteration or lava apophyses); one exception is alteration of these deposits around a ~6 m thick laccolith composed of multiple sills. On the accessible upper flanks (the Chufquén and East valleys: Fig. 2c), the sills are more continuous, sometimes thicker, and some intrude the lower parts of the debris flow subsequence, roughly parallel to the slope and bedding of the deposits (sometimes with alteration haloes); examples are shown in Fig. 8. Dykes are also present in this subsequence, most notably some of distinct composition that clearly feed the circum-caldera lavas, which are surrounded by prominent alteration zones (e.g., Fig. 7c). Groups of cross-cutting dykes with no clear association are also recognised, most clearly in the Chufquén valley (Fig. 8c), where there is also an atypical large intrusion capping the subsequence (Fig. 4f).

3.3. Chufquén valley lavas

The upper Chufquén valley (Fig. 2c) contains several lava units, ranging from tens to hundreds of metres in length and ~3–15 m in thickness, with a variety of morphologies. Their age is currently unconstrained, except by the fact that they post-date the erosion of the Chufquén valley, and so the Sharkfin sequence. The lavas analysed chemically are all of near-identical basaltic andesite composition, but less alkalic for their silica content than almost all the samples from other units (Fig. 3). Therefore, it is unclear how they relate to the main stratigraphy. Examples of the significant features of these lavas are shown in Fig. 9. Some show entablature (e.g., Long and Wood, 1986; Forbes et al., 2014a) on the steep valley-facing sides of the flows; cube, curvi-columnar, chevron-like, and irregular fractures are all observed, bounded by either blocky fracturing or a colonnade of columnar jointing (Figs. 9a and 9b). Hackly fractures are present at the margins of other flows (Figs. 9d and 9e); these locally have curving chisel marks (striae) on their surfaces (Figs. 9e and 9f). The other lavas show no pervasive fracturing, only typical marginal

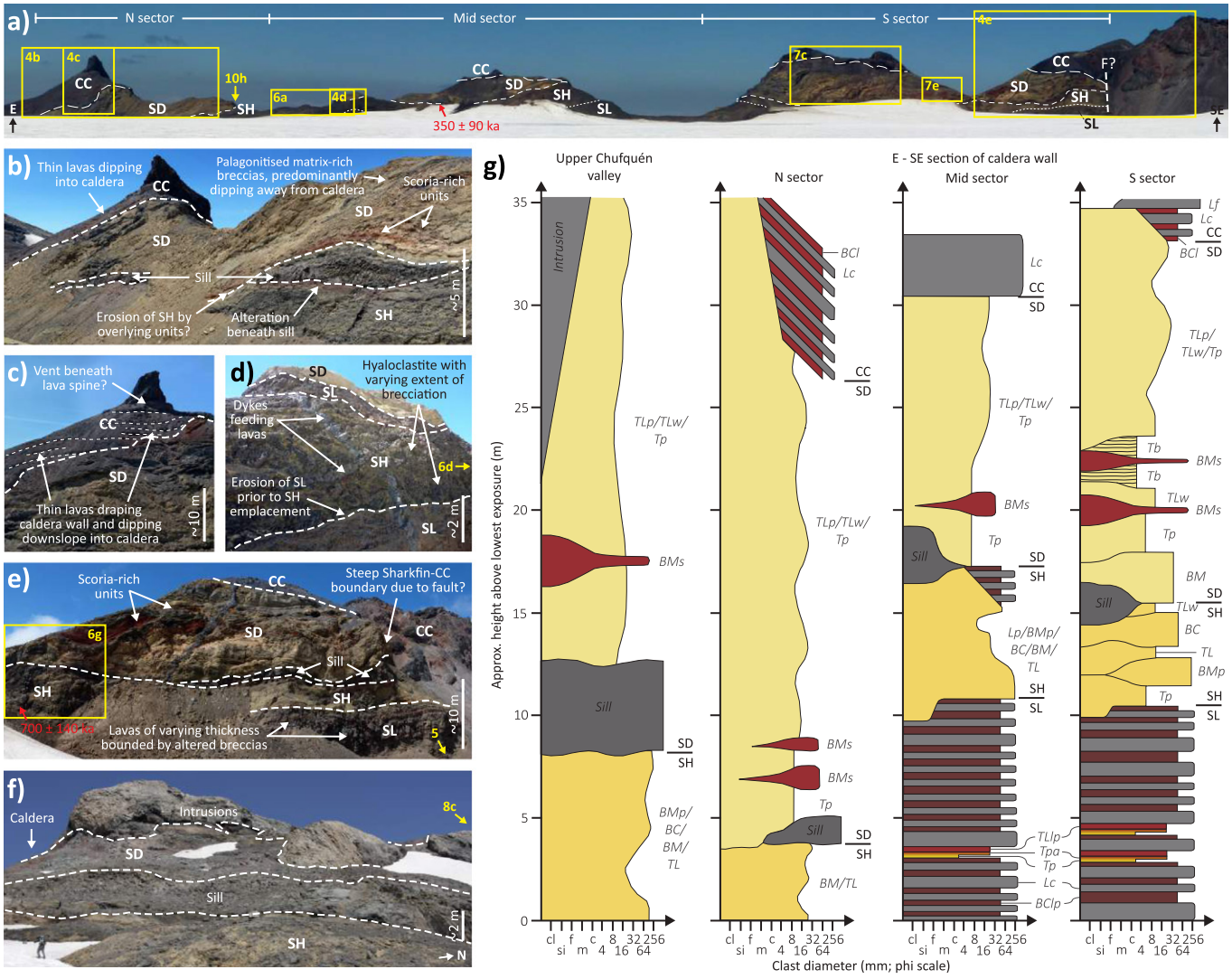

Fig. 4. Overview of the stratigraphy of the pre-caldera 'Sharkfin' sequence (Section 3.2) and part of the overlying circum-caldera lava sequence (Section 3.4), which shows the consistent nature of the general stratigraphy where these units are exposed around the caldera. In Parts a to f, most dashed lines approximately delineate the contacts between different subsequences (labelled), the yellow boxes and arrows indicate the extent and/or location of sections of the caldera wall shown in other figure parts, and the red arrows point to the location of dykes that have been Ar–Ar dated to the stated ages (Supplementary File 2; Section 3.2.2). (a) Panorama of the E to SE section of the caldera wall (marked on Fig. 2b), showing most of the key outcrops of the Sharkfin sequence. (b) Outcrop of the middle to upper part of the Sharkfin sequence, overlain by circum-caldera lavas dipping both into and out of the caldera. (c) Alternate view of the circum-caldera lavas shown in Part b. (d) Outcrop of the lower to middle part of the Sharkfin sequence, including the lava subsequence capping the hyaloclastite subsequence, which is uncommon. (e) Outcrop of all the main parts of the stratigraphy in this section of the caldera rim. (f) View of the west side of the uppermost Chufquén valley (Fig. 2c), where the middle to upper part of the Sharkfin sequence is also exposed. (g) Generalised and simplified vertical profiles for the sections of the caldera wall where the Sharkfin sequence is present. The (sub)sequence (bold) and lithofacies (italic) codes correspond to those in Table 2. Note that the clast size variations within each subsequence are representative of their range and variability, but are not based upon a specific vertical section as there is no consistent internal stratigraphy.

autobreccia (Fig. 9c). There is no clear pattern to the distribution of lavas with each particular morphology.

3.4. Circum-caldera lava sequence

This sequence comprises the lavas that cap the majority of the caldera walls, including those in the eastern sector that overlie the Sharkfin sequence (Fig. 4a); it post-dates the formation of the caldera. The lavas are basaltic andesite to trachydacite in composition and contain varying concentrations of phenocrysts (plagioclase, one or two pyroxenes, olivine, and/or Fe–Ti oxides). The sequence includes the Peak and South units of Gilbert et al. (1996), which are grouped together in this study due to their very similar geochemistry (Murphy, 1996). At a few locations on the eastern caldera wall, at the base of this sequence there are thin (<2 m thick) 'a'ā lavas (Fig. 4), which have been inferred to be subaerial (Gilbert et al., 1996). Previous work (Gilbert et al., 1996; Murphy, 1996) considered these lavas the uppermost part of the pre-caldera Sharkfin sequence. However, this is inconsistent with the orientation of some of these lavas, dipping both to the north and into the caldera (Figs. 4b and 4c), and the trachydacite composition of those sampled (Murphy, 1996), given that the Sharkfin sequence is otherwise exclusively mafic (Fig. 3). Hence we consider these part of the circum-caldera lavas, despite being morphologically distinct from the lavas that otherwise form the lower part of this sequence.

The bulk of the sequence comprises lava domes/coulées and stacks of flows, ~10–100 m in height and width on the caldera rim; examples are shown in Fig. 10. There is a transition in the morphology of the lavas at approximately the same elevation around the eastern and southern caldera rim (Fig. 10a). Below this level there are steep caldera-facing cliffs of lava, comprising both thick (>10 m) flows (e.g., Fig. 10f) and sides of domes/coulées (e.g., Fig. 10c). These cliffs are pervasively fractured in one or more patterns such as columnar, hackly, and

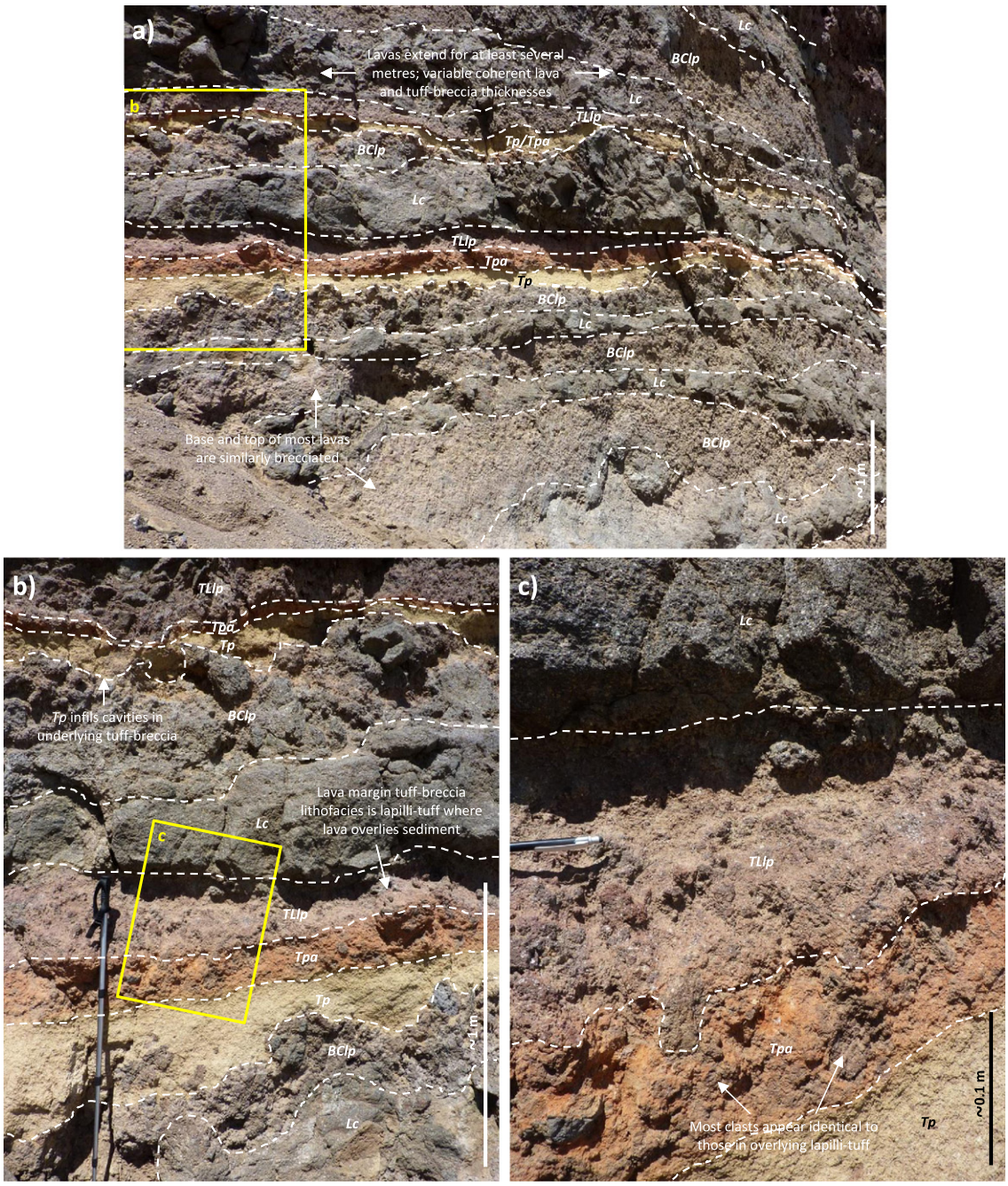

Fig. 5. Photographs of a caldera-rim outcrop of the Sharkfin lava subsequence (located where indicated in Fig. 4e), which show the main features of this subsequence described in Section 3.2.1, and the constituent lithofacies described in Table 2 (the lithofacies (italic) codes correspond to those in Table 2). The dashed lines delineate the approximate boundaries between lithofacies. The yellow boxes indicate the approximate areas magnified in other photographs. (a) Part of the outcrop, showing multiple tuff-breccia-enclosed lavas and two interspersed palagonitised tuff units. (b) and (c) Closer views of a section of Part a, which show the relationships between the constituent lithofacies in more detail. Note that the lava margin tuff-breccia *TLlp* shown in Part c is an atypical lithofacies that is only present where a lava unit overlies a palagonitised tuff unit.

pseudopillow (summary definitions in Lescinsky and Fink, 2000) (e.g., Figs. 10b and 10g), or occasionally radial (Fig. 10e). All these lava cliffs were not accessible for detailed characterisation. There are occasional lavas that flowed into the caldera from the cliffs; these lavas are particularly densely fractured (Figs. 10d and 10g). In some instances this fracturing is platy, i.e., sub-parallel and spaced <10 cm apart, and sometimes curving (e.g., Fig. 10b) or sub-parallel to flow direction (inferred from flow banding and/or morphology, e.g. Fig. 10d). We also find platy fracturing on one margin of the dyke forming one side of the head of the East valley (Fig. 2c): as shown in Fig. 10h, the valley-facing margin of the dyke has a strong curved platy fabric, with horizontal columnar jointing (i.e., polygonal in a plane parallel to the dyke margin) just behind, whilst the other margin, in contact with Sharkfin palagonitised lapilli-tuff, is fractured into large blocks. Some of the dykes feeding the circum-caldera lavas (in the Sharkfin sequence exposed at the caldera walls) show cube-like fracturing, and columns oriented parallel to the dyke margins (rather than perpendicular, which is expected as a dyke cools from its margins) (Figs. 7c and 10c).

Above the aforementioned level on the caldera rim, there are stacks of thinner (<5 m thick), less fractured ʻaʻā lavas, sometimes with oxidised margins (e.g., Figs. 10f and 10g). These lavas form the Peak unit described by Gilbert et al. (1996), who report that they dip both

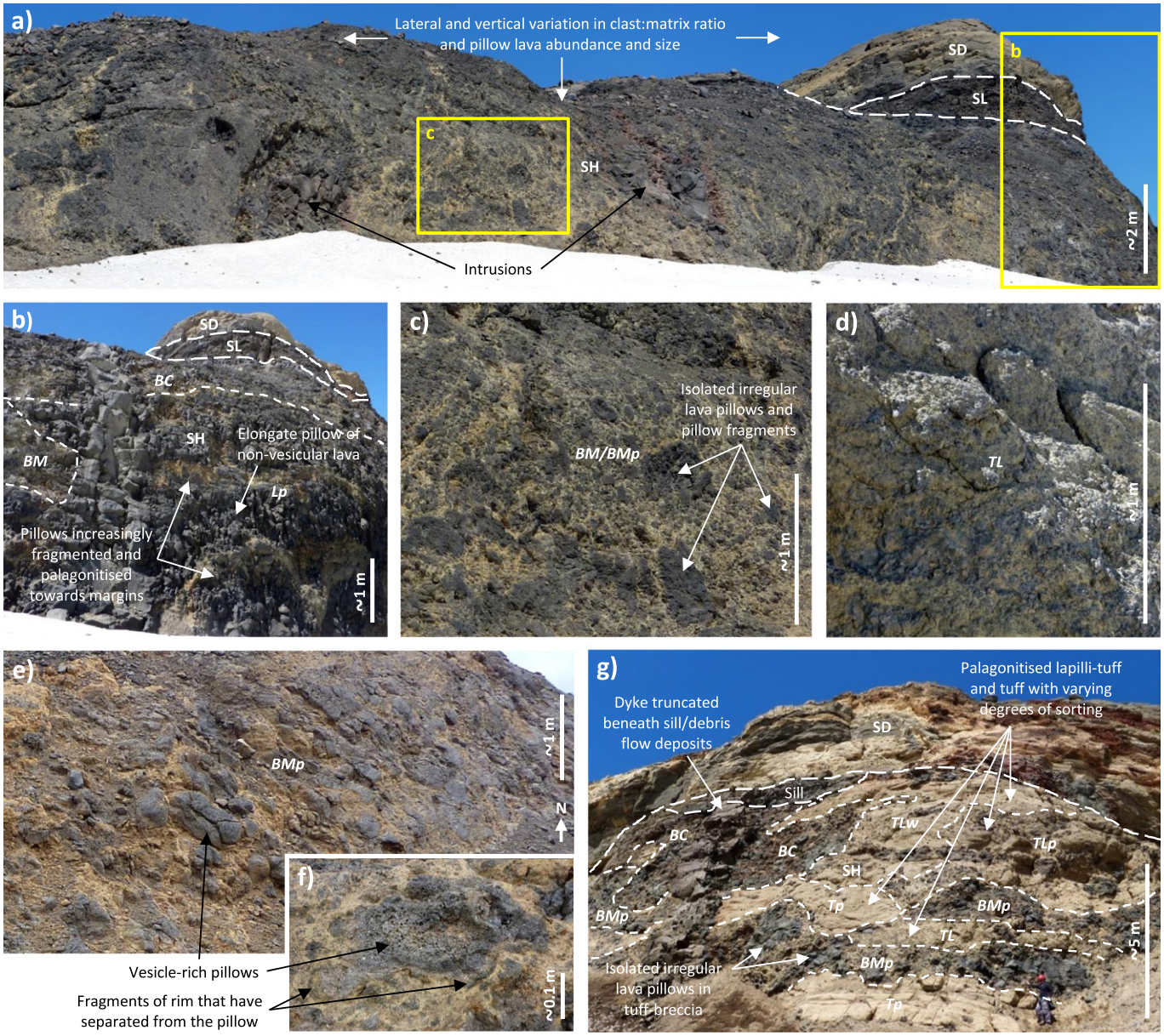

Fig. 6. Photographs of outcrops that exemplify features of the Sharkfin hyaloclastite subsequence that are described in Section 3.2.2, and show the constituent lithofacies described in Table 2 (the (sub)sequence (bold) and lithofacies (italic) codes correspond to those in Table 2). The short-dashed lines approximately delineate some of the different lithofacies; the longer dashed lines approximately delineate subsequence boundaries. (a) A caldera-rim outcrop (approximately demarcated in Fig. 4a), showing the metre-scale variations in pillow size/shape and content, clast size, and clast:matrix ratio (and so lithofacies) and absence of a consistent stratigraphy, which are typical of the subsequence. The yellow boxes indicate the approximate areas magnified in the subfigure specified. (b, c, d) Closer views of caldera-rim outcrops (Part d is located where indicated on Fig. 4d) showing sections of the spectrum of hyaloclastite textures, from lava pillows with fragmented margins (Part b) through pillow fragment tuff-breccia (Part c) to block- and then lapillus-sized angular to subrounded lava fragment tuff-breccia and lapilli-tuff (Part d). (e) An outcrop in the upper Chufquén valley (Fig. 2c) showing relatively small, vesicular, and rounded lava pillows isolated within palagonitised lapilli-tuff. (f) A single pillow in the same unit as the outcrop in Part e, which shows the vesicularity of the lava and a fragmented rim that has separated from the pillow. (g) A caldera-rim outcrop (approximately demarcated in Fig. 4e) where this subsequence (atypically) comprises lenses/sheets of tuff-breccia (mostly pillow-bearing) within palagonitised tuff and lapilli-tuff.

into and out of the caldera, and include an unusually large, ~2 km long fractured lava (geochemically distinct according to Murphy, 1996) that flowed into and across the northwest part of the caldera. The flank-facing sides and top of the lava domes/coulées in the sequence are blocky or weathered (e.g., Figs. 10b and 10e), less steep than the caldera-facing sides, and sometimes oxidised; some of the coulées have associated lavas that extend up to hundreds of metres down the flanks (e.g., Fig. 8a). The brecciated, oxidised carapaces suggest that the domes/coulées have not been substantially eroded, and thus that the exposed faces are the actual dome margins (Gilbert et al., 1996). The largest stacks of lavas (on the southern caldera rim; Fig. 10a) are morphologically very similar to lava-dominated flat-topped or conical tuyas (Russell et al., 2014), at least on their caldera-facing sides.

Groundmass samples of two of the aphyric lava domes on the eastern caldera rim (marked on Fig. 10) have been Ar–Ar dated by the method outlined in Arancibia et al. (2006) to 26 ± 5 and 68 ± 14 ka (Supplementary File 2), coinciding with the LGM and a proposed Southern Hemisphere glacial maximum (~65 ka; Schaefer et al., 2015) respectively. The younger date is probably not robust as it is close to the limit of the dating method; the elder is consistent with the Ar–Ar date of 64 ± 15 ka obtained for a circum-caldera sequence lava on the NW caldera rim by Jara and Moreno (in preparation) (Table 1).

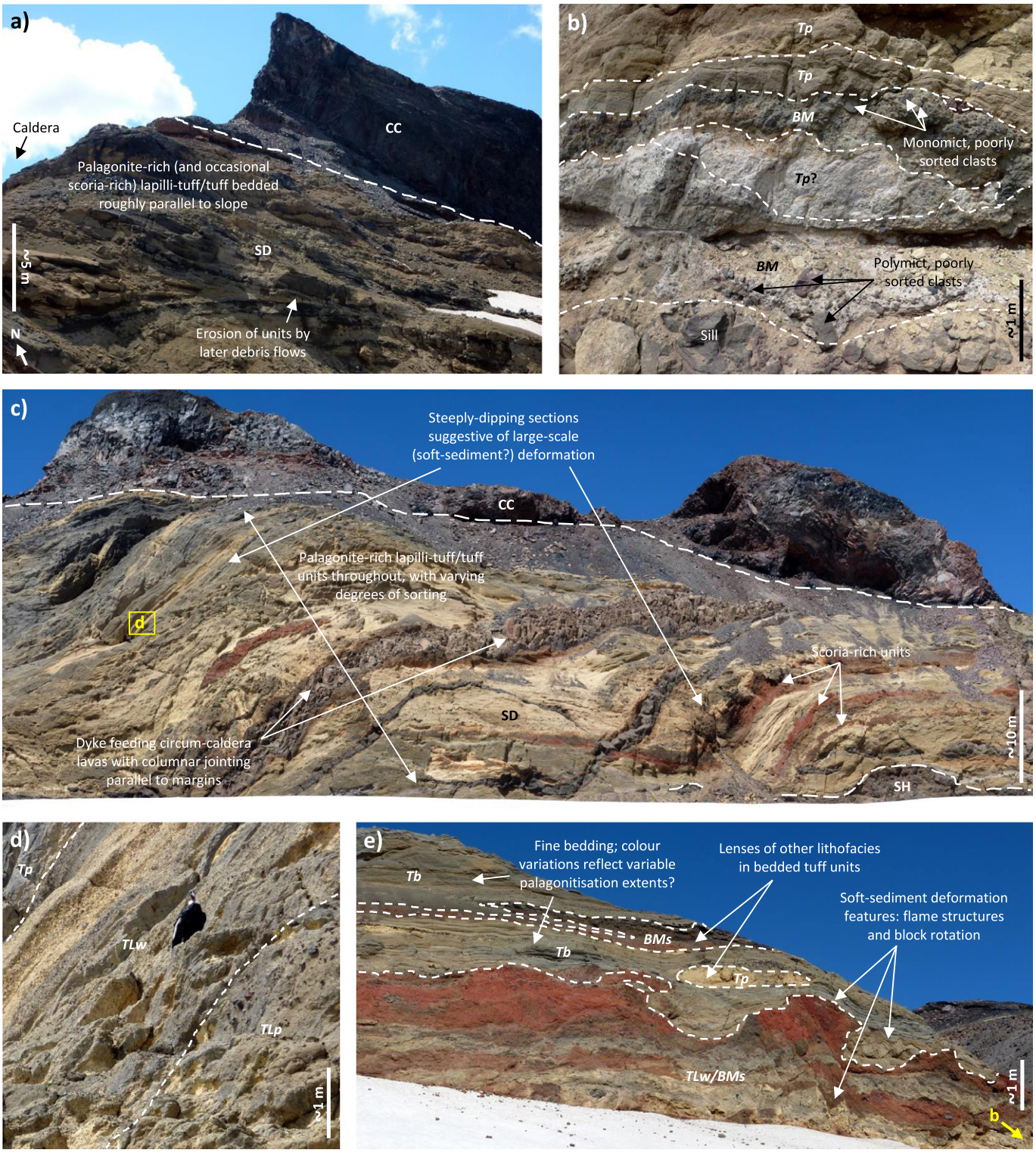

Fig. 7. Photographs of outcrops that exemplify features of the Sharkfin debris flow subsequence that are described in Section 3.2.3, and of some of the constituent lithofacies described in Table 2 (the (sub)sequence (bold) and lithofacies (italic) codes correspond to those in Table 2). The short-dashed lines approximately delineate some of the different lithofacies or units; the longer dashed lines approximately delineate subsequence boundaries. (a) View of the north side of the uppermost part of the East valley (Fig. 2c), which shows the slope-parallel stratigraphy of some units of the debris flow subsequence (observed in the caldera walls in Fig. 4b). (b) A caldera-rim outcrop (located where indicated on Fig. 7e) showing examples of the tuff-breccias and palagonitised tuffs that are respectively sometimes and often present at the base of the subsequence. Note the channelised distribution of some of the units, which are defined by abrupt changes in colour and/or texture, and so even those with the same lithofacies classification are distinguishable. (c) A caldera-rim outcrop (approximately demarcated in Fig. 4a) predominantly showing palagonitised tuff/lapilli-tuff lithofacies typical of the middle and upper parts of the subsequence, and examples of the large length-scale deformation present in parts of this subsequence. The yellow box indicates the approximate area shown in Part d. (d) View of some of the (inaccessible) units typical of the upper part of this subsequence, showing that they comprise variably sorted, palagonitised lapilli-tuff and tuff. (e) A caldera-rim outcrop (approximately demarcated in Fig. 4a) showing the scoria-bearing and variably palagonitised lapilli-tuff/tuff units in this subsequence, and examples of the smallest-scale soft-sediment deformation present.

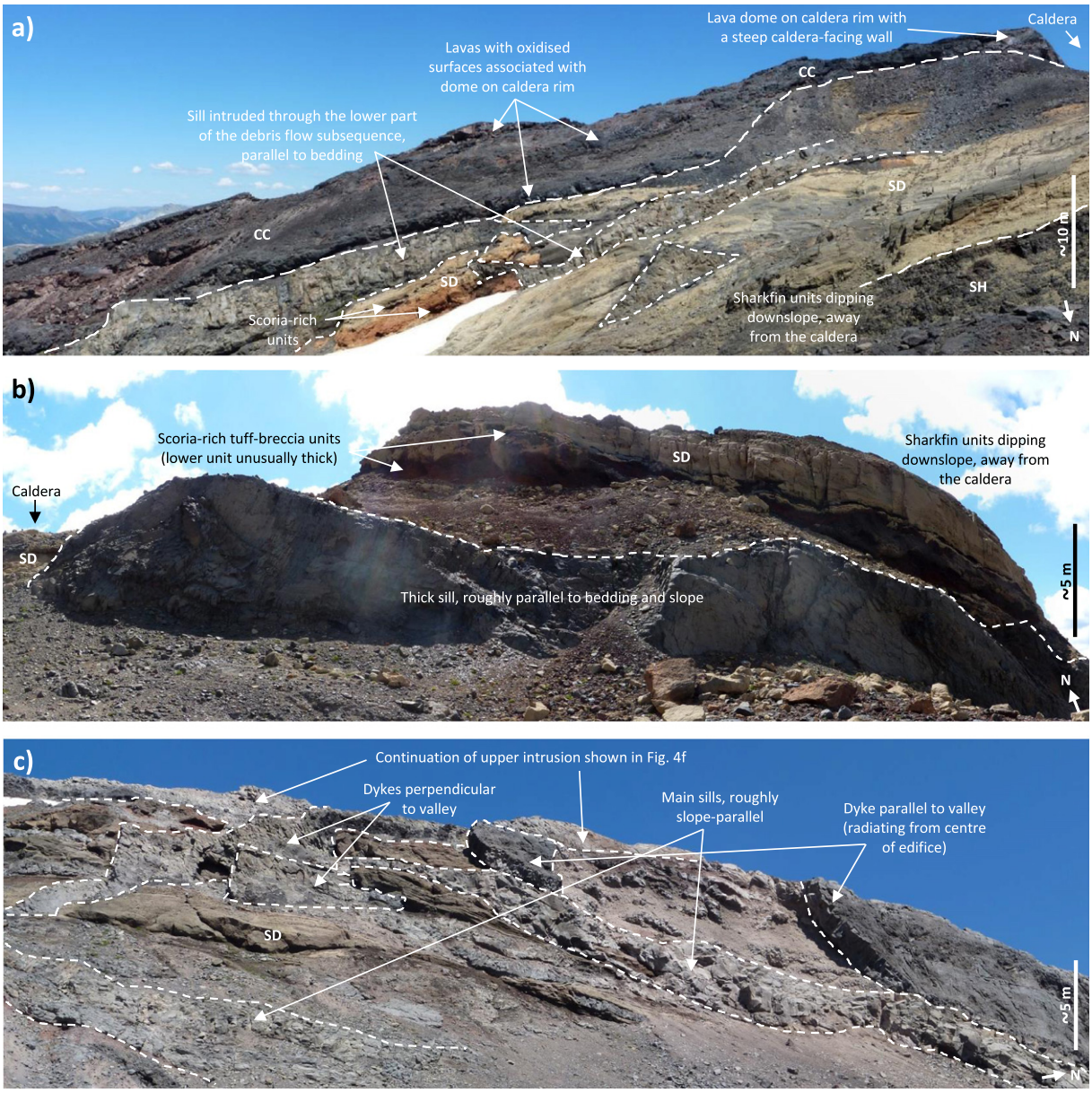

Fig. 8. Photographs showing the extent and variety of some of the intrusions in the upper part of the Sharkfin sequence, which are discussed in Section 3.2.3. The short-dashed lines approximately delineate the intrusions and the longer dashed lines approximately delineate subsequence boundaries; the subsequence codes are defined in Table 2. (a, b) Views of the south (Part a) and north (Part b) sides of the uppermost East valley (Fig. 2c), which show the downslope continuation of the stratigraphy observed in the caldera walls, including the sills at/near the base of the debris flow subsequence. Note that only the lower parts of the debris flow subsequence are present here and in the corresponding sector of the caldera wall (the mid sector in Fig. 4a). (c) View of the west side of the Chufquén valley (Fig. 2c; downslope from Fig. 4f), showing sills at/near the base of the debris flow subsequence and additional intrusions further up the stratigraphy.

4. Interpretation and discussion of eruptive and glacial history

4.1. Sharkfin sequence

4.1.1. Sharkfin lava subsequence

The environmental conditions in which this subsequence was emplaced are unclear. The lavas are more brecciated than typical subaerial basaltic 'aʻā flows, and the matrix of the tuff-breccia units shows uniform partial palagonitisation, suggesting meltwater was present during their emplacement. We suggest that the well-sorted palagonitised tuff units interbedded with the lavas result from reworking of subaqueous/subglacial eruption deposits, and so indicate at least intermittent water flow. Nevertheless, the extent of fragmentation and palagonitisation of the lavas is much less than that in typical subaqueous or subglacial fragmental lithofacies (cf. the hyaloclastite subsequence), and the fracturing within the coherent lava is irregular, rather than of a pattern indicative of snow (e.g., Mee et al., 2006) or ice (e.g., Lescinsky and Fink, 2000) contact. Glacial evidence for coeval ice is not observed, although it is not possible to rule out the presence of striations on the lavas or basal diamict from the outcrops studied. The occasional presence of this subsequence overlying the hyaloclastite subsequence could be interpreted as an indication that these lavas can result from eruption into drained subglacial cavities. Given this association, we suggest that this subsequence results from a succession of lava flows beneath snow or ice from which the meltwater generated was able to drain rapidly; the snow/ice thickness required is

impossible to constrain beyond that it must exceed that of the subsequence (>11 m). However, subaerial emplacement cannot be ruled out.

4.1.2. Sharkfin hyaloclastite subsequence

The lithofacies in this subsequence are similar to some of those inferred to result from mafic eruptions beneath ice (e.g., Loughlin, 2002; Schopka et al., 2006) or water (e.g., Porębski and Gradziński, 1990; Watton et al., 2013); the ubiquitous palagonitisation of the fine-grained glass component of each lithofacies is consistent with a hyaloclastic origin (e.g., Fisher and Schmincke, 1984). Topographic features such as craters and moraines can reduce the local slope and/or enable local thickening of ice cover, and so encourage meltwater ponding even on the slopes of a stratovolcano; substantial meltwater accumulation has been reported within large craters or calderas (e.g., the 1991 eruption of Volcán Hudson, Chile: Naranjo et al., 1993b) (Lescinsky and Fink, 2000). However, this subsequence is probably too extensively distributed in a consistent stratigraphic position to be accounted for by such localised ponding. We consider the most plausible formation mechanism for this subsequence to be effusive mafic eruptions beneath ice of sufficient thickness that it has surface topography independent of that of the land surface (the former being a more effective control on meltwater flow: Björnsson, 2002), and so able to create a 'hydraulic seal' that hinders drainage of meltwater generated by the eruption (Björnsson, 2002; Stevenson et al., 2009). Under such conditions, meltwater would have ponded in subglacial cavities and so been available to interact with the lava; water retention is only required for the duration of the eruptive phase. Stevenson et al. (2009) suggested that ice in excess of 300 m thick may be required to pond meltwater subglacially on steep topography. However, it is not possible to definitively constrain the absolute ice thickness range under which this subsequence could

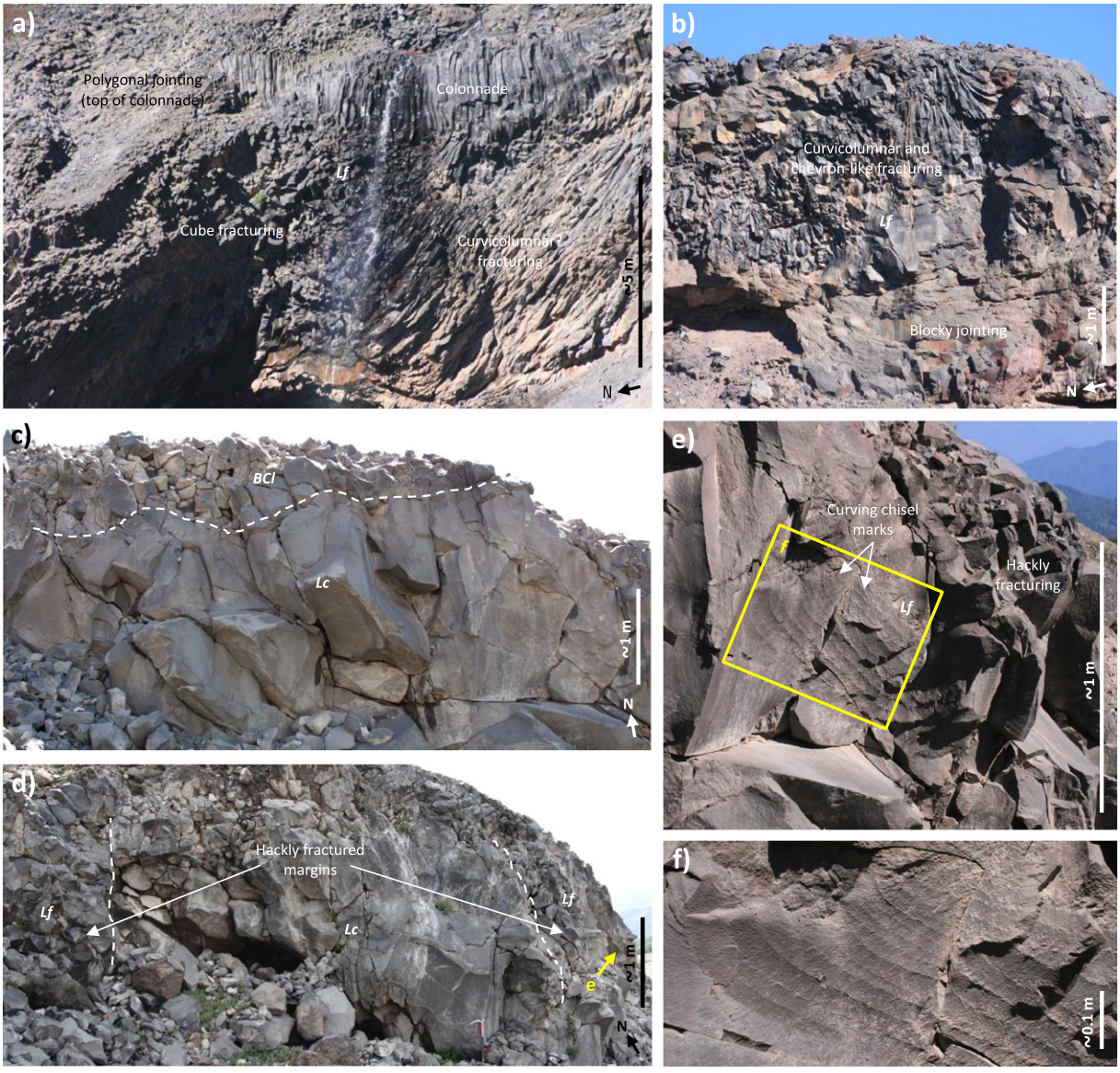

Fig. 9. Photographs of outcrops that exemplify features of the lavas within the upper Chufquén valley, described in Section 3.3. The dashed lines approximately delineate the different lithofacies, the codes for which correspond to those in Table 2. (a) Outcrop of the valley-facing side of a thick lava that flowed from near the caldera rim, showing a pervasively fractured centre (entablature) capped by a colonnade. (b) Outcrop of a smaller lava on the valley floor, which also shows entablature-like fracturing. (c) Outcrop of a lava in the valley floor, in which pervasive fracturing is absent. (d) Outcrop of a lava in the valley floor (further downslope than the lava in Part c) with hackly fracturing at its margins. (e, f) Detail of part of the margin of the lava in Part d (areas indicated by the yellow arrow in Part d and approximately demarcated by the yellow box in Part e, respectively), showing the jointing and prominent curving chisel marks on some surfaces.

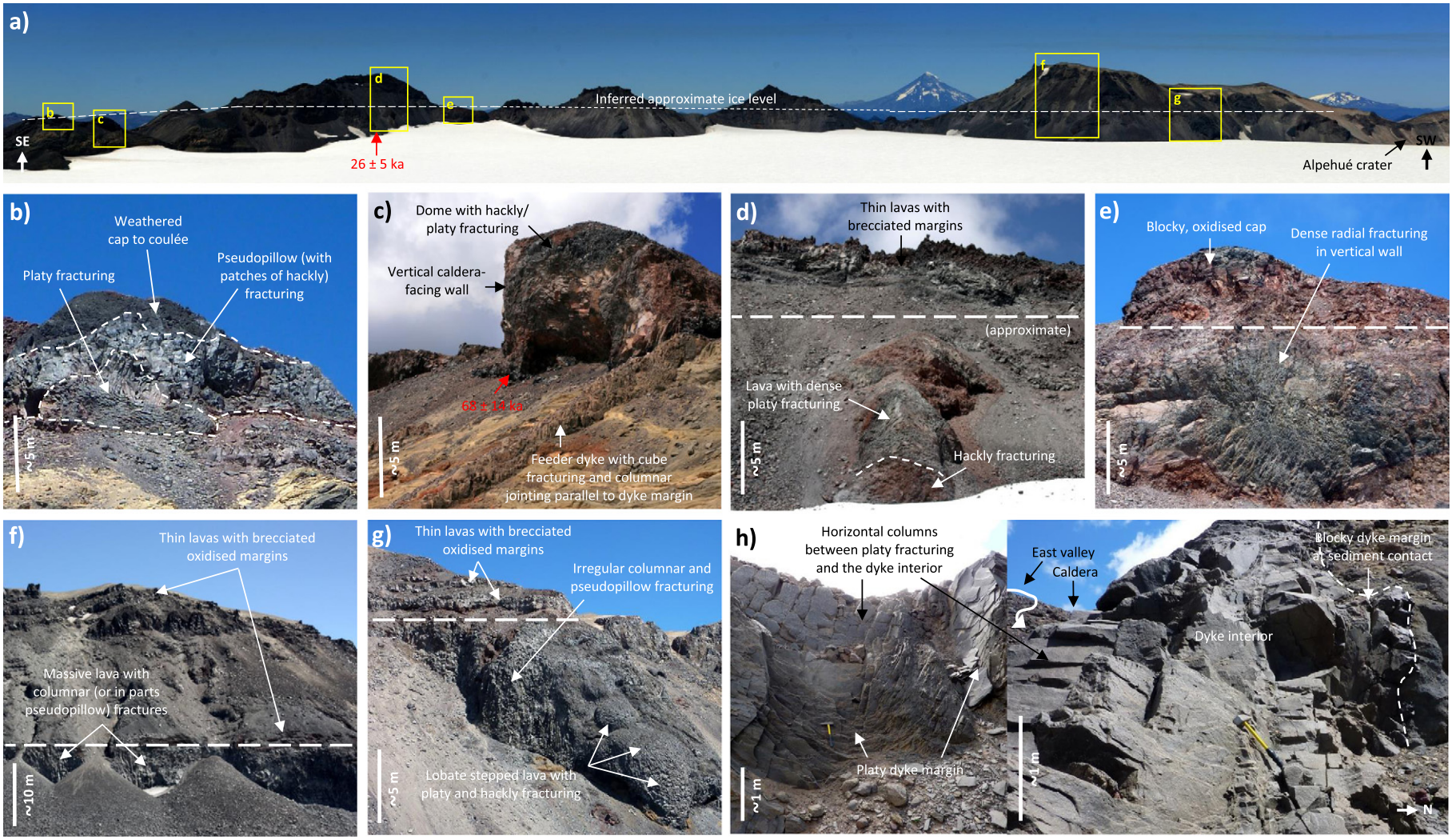

Fig. 10. Examples of the morphologies observed in the circum-caldera lava sequence and intrusions discussed in Section 3.4, and the consequent inference of syn-eruptive ice extent or thickness. The red arrows point to the sampling locations of lavas that have been Ar–Ar dated to the stated ages (Supplementary File 2; Section 3.4). (a) Panorama of the SE to SW sector of the caldera wall (marked on Fig. 2), which predominantly comprises lavas of the circum-caldera lava sequence. The dashed line indicates the approximate level below which there are morphological features interpreted as evidence of interaction with ice/meltwater, and so is the inferred ice level during lava emplacement; longer dashes denote where this is better constrained. The yellow boxes indicate the parts of the caldera wall shown in Parts b to g, which, together with Part h (the location of which is indicated on Fig. 4a) are examples of the morphological features and how the palaeoice level has been delineated. (b) Near-vertical caldera-facing wall to a lava coulée on the caldera rim, which displays a variety of fracturing types (labelled) that are perhaps indicative of rapid cooling due to ice contact (e.g., hackly and pseudopillow fracturing: Lescinsky and Fink, 2000), suggesting that the coulée was buttressed by intra-caldera ice on emplacement. (c) A lava dome on the caldera rim with a near-vertical caldera-facing wall, displaying similar fracturing types. Columnar jointing of the exposed feeder dyke parallel to its margins indicates cooling from the surface rather than the dyke margins, suggesting attempted intrusion into intra-caldera ice. (d) Lava that flowed down the caldera wall from near the top, with pervasive platy fracturing that might reflect emplacement along the ice–rock interface (cf. Part h), overlain by typical (subaerial) ʻaʻā lavas. (e) Lava with a vertical, radially fractured caldera-facing wall, capped by a more oxidised, blocky carapace, perhaps either a cross-section of a lava tube or a small coulée that was constrained by intra-caldera ice (cf. Edwards and Russell, 2002). (f) A steep caldera-facing wall of columnar-jointed lavas, perhaps emplaced against intra-caldera ice, overlain by a thick sequence of typical (subaerial) ʻaʻā lavas. (g) Lava lobes with hackly and platy fracturing from a steep-sided lava with irregular columnar fractures, which is overlain by typical (subaerial) ʻaʻā lavas. The lobes are interpreted to have flowed into cavities melted in the intra-caldera ice that confined the lava cliff. (h) Dyke with blocky fracturing on its northern margin, where in contact with debris flow units of the Sharkfin sequence, and pervasive platy and polygonal fracturing along the south margin (shown in the left-hand photograph), where facing the dyke-parallel East valley (Fig. 2b) that intersects the caldera rim. The different fracture patterns on the two sides are interpreted to have formed by the dyke intruding along the interface between the sidewall and ice infilling the valley.

have formed without the preservation of any clear transition to subaerial activity (as identified where the emplacement conditions of similar deposits have been constrained, e.g. Brown Bluff volcano (Smellie and Skilling, 1994)). Although the ice must have been at least as thick as the deposits, at a maximum of ~12 m, this is at least an order of magnitude too thin to be a reasonable lower bound on the ice thickness.

The spectrum and spatial relationships of the lithofacies identified in this subsequence could be generated in various ways in this subaqueous/subglacial regime. If explosive fragmentation was the predominant mechanism of brecciation of the erupted lava, then spatiotemporal variation in the subglacial cavity pressure, determined by the rates of meltwater generation and discharge, would likely be the main control (lower cavity pressure allowing greater explosive fragmentation, and vice versa) (Tuffen, 2007). However, we suggest that this is inconsistent with the absence of systematic trends in fragmentation extent through the subsequence, or any correlation between fragmentation extent and the vesicularity of the lava component. Passive quench and mechanical fragmentation, to which hyaloclastite formation is attributed by studies such as Skilling (2002; 2009) and Watton et al. (2013), is suggested to be the predominant mechanism by: (1) the increasing fragmentation of lava pillows towards their margins, (2) the clast-rich, sometimes isolated pillow-bearing, and poorly sorted nature of many of the tuff-breccias, and (3) indications of slumping and/or remobilisation (e.g., the occasional lenses or sheets of one tuff-breccia or tuff/lapilli-tuff lithofacies within another), which can induce mechanical fragmentation (Skilling, 2002). Such fragmentation may have been driven by long-lived extrusion on a steep slope, encouraging slumping downslope, analogous to the formation of poorly bedded hyaloclastite foresets in ‘a‘ā lava deltas (Smellie et al., 2013, 2014). The formation of a particular hyaloclastite lithofacies will therefore depend on factors including the eruption/lava flow rate, magma–water interaction efficiency, timing and rate of meltwater discharge, and topography, all of which are likely to be highly spatially and temporally variable, consistent with the observed stratigraphy.

4.1.3. Sharkfin debris flow subsequence

The mix of channelised and sheet deposits (sorted to varying extents, some polymictic) in this subsequence indicates that it was formed by a series of debris flows of varying energy. Most of the subsequence comprises rocks very similar to those in the hyaloclastite subsequence (but with textural differences, e.g. bedding and clast:matrix ratio), suggesting that these flows likely reworked deposits from subglacial eruptions. The scoria-bearing and bedded tuff units are also probably remobilised (from subaerial or subaqueous explosive eruption deposits), because they are typically found mixed with or containing lenses of breccia and are highly variable in thickness. The consistent stratigraphic position of the widely distributed pair of oxidised scoria-bearing units suggests that at least the lower units of this subsequence were emplaced approximately contemporaneously. The extensive distribution of this part of the subsequence therefore implies that it was formed by discharge of a large volume of water. It is unlikely that such a volume could have been generated by local meltwater ponding, so we suggest that it may have originated from eruptions beneath a thick ice sheet (for reasons discussed in Section 4.1.2).

The association of sills and a thick sequence of debris flows is similar to the Dalsheidi-type subglacial volcanic sequences in southern Iceland described by Smellie (2008). These comprise a semi-continuous lava sheet (sometimes underlain by diamict) with columnar jointing and/or entablature, which partially intrudes into overlying massive sheet-hyaloclastite (sometimes capped by mudstone) (Smellie, 2008). These sequences can range from <5 m to hundreds of metres in thickness (where multiple sequences are present in succession) and extend many kilometres from their source. One interpretation is that they are produced by a sill intruding along the bedrock–ice interface beneath a thick temperate ice sheet, which generates sufficient meltwater to eventually float the ice sheet, causing a debris flow of hyaloclastite (erupted at the vent) beneath it (Smellie, 2008). Alternatively, Banik et al. (2014) argue that these sequences are the result of eruptions beneath thin or negligible ice (supported by measurements of the volatile content of glass), with the ‘sills’ being lava flows that either preceded the debris flows or intruded down into and along the base of pre-existing deposits. We suggest that the sills and debris flow deposits described here were emplaced beneath thick ice, in a similar way to the model of Smellie (2008). This is because the sills appear to have intruded along the base of the ice both prior to and during the debris flows (as they are present both beneath the subsequence, with no alteration of the overlying deposits, and in its lower parts, mostly parallel to the bedding), contradicting the models of Banik et al. (2014). Furthermore, it is difficult to reconcile the apparently contemporaneous deposition of the sequence of debris flows as extensively as they are present on Sollipulli with the amount of meltwater that could be generated beneath thin glaciers. Analysis of the volatile content of the sills (Dixon et al., 2002; Tuffen et al., 2010) would be necessary to verify this interpretation. Constraint of the absolute ice thickness range under which this subsequence could have formed is not possible, due to the absence of a contemporaneous subaerial cap, but it is likely to be greater than that which resulted in the hyaloclastite subsequence, considering the greater meltwater volume required in this instance.

4.2. Chufquén valley lavas

We interpret these lavas to have been emplaced in a variety of environmental conditions. Entablature is diagnostic of rapid cooling due to water infiltration (e.g., Long and Wood, 1986; Forbes et al., 2014a); the (sub-)vertical fracturing orientation in the lavas with this feature suggests that this cooling resulted from flooding during emplacement, rather than ice interaction at their margins. However, the hackly fracturing (also symptomatic of rapid cooling: Lescinsky and Fink, 2000) at the margins of other lavas suggests that such ice contact occurred in the case of these other units. With further examination, the chisel marks on the fracture planes would have the potential to constrain the cooling front and rate (e.g., DeGraff and Aydin, 1987; Goehring and Morris, 2008; Forbes et al., 2012). Other lavas lack such features, and are hence inferred to be subaerial; some of these are upslope of those with fracturing indicative of ice interaction, so the glaciation extent when the suite of lavas was emplaced is unclear. We propose that they erupted over a protracted period during which the glacier size changed. Note that none of these lavas are pervasively fragmented, nor is there evidence of palagonitisation, in contrast to the Sharkfin sequence despite also being of mafic composition; this most likely reflects a difference in the amount of meltwater interaction due to ice thickness.

4.3. Circum-caldera lava sequence

The morphologies and fracture patterns observed on the caldera-facing sides of these lavas suggest that when the bulk of this sequence was erupted at the top of the caldera wall, the lavas were constrained on this side by intra-caldera ice, similar to, for example, the perched lavas at Mt Rainier (Lescinsky and Sisson, 1998) and ice-dammed lava cliffs at Hoodoo Mountain (Edwards and Russell, 2002). Some lava breached out of this dammed lava and flowed into the caldera along the ice–rock interface (i.e., subglacially); we interpret their densely fractured surfaces as a reflection of the resulting enhanced meltwater interaction. Some of the lavas display multiple fracture patterns; previous studies have attributed these to cooling rate variation with distance from the ice contact (e.g., Lodge and Lescinsky, 2009). When the lavas built up to ice level, extrusion continued subaerially (forming the caps of the domes and the thin ‘a‘ā lavas); lava may have flowed over the intra-caldera ice, but only the parts of lavas on the caldera rim have been preserved.

Two of the types of fracturing observed in the lower-level lavas are not commonly associated with ice interaction. Radial fracturing is one of these; the example shown in Fig. 10e could be interpreted as a cross-section of a lava tube rather than the ice-constrained margin of a thick flow, although the fractures are closely spaced, consistent with rapid cooling, and radial fracturing has also been interpreted as indicative of lava-ice contact at some other stratovolcanoes (e.g., Hoodoo Mountain: Edwards and Russell, 2002). The other, platy fracturing, is found in lavas erupted under various conditions, but typically only in the slowly cooled interior of lavas (Lescinsky and Fink, 2000), whether they are subaerial (e.g., Tuffen et al., 2013), ice-contact (e.g., Mee et al., 2006), or subglacial (e.g., Forbes et al., 2014b). Conversely, in this sequence platy fracturing is present on the surface of lavas (Fig. 10d) and the same caldera-facing lava cliffs as patterns indicative of rapid cooling, such as hackly fracturing (Figs. 10b and 10g). We suggest that the platy fracturing on one surface of the dyke shown in Fig. 10h arises from its intrusion along the contact between a glacier in the valley and the valley side, causing rapid cooling of the dyke margin in contact with the ice. Therefore, we propose that platy fracturing can result from ice interaction (e.g., in the case of the lava shown in Fig. 10d); it perhaps forms when the lava or dyke margin is rapidly cooled into the brittle regime but the interior is still undergoing ductile flow, causing a shear fabric to form in the margin. Formation mechanisms for platy fractures in the interior of lavas proposed by previous studies include late-stage shear (Bonnichsen and Kauffmann, 1987; Conway et al., 2015) and detachment of the outer parts of the lava body, possibly due to deflation (Spörli and Rowland, 2006) or inflation (Tuffen et al., 2013). However, the presence of undeformed master fractures cross-cutting the curved platy interior fractures in the subglacial lava studied by Forbes et al. (2014b) was interpreted to indicate that such fracturing is unlikely to form by inflation, deflation, or late stage shear, and so perhaps by cooling contraction instead. Conversely, modelling of the cooling of an andesite lava by Spörli and Rowland (2006) suggested that chilling alone could not reasonably account for the longitudinal strain across platy fractures, suggesting a mechanical component.

The approximately consistent elevation (~2100 m) of the ice-interaction to subaerial transition in the caldera-facing lavas indicates that the bulk of this sequence was emplaced during a period when the caldera was filled with ice. There are several hanging valleys in the caldera rim below the inferred ice level (Figs. 4a and 10a), so an ice accumulation rate in excess of that of drainage by outlet glaciers would have been necessary to reach this level. The subaerial lavas flowing into the caldera that are locally present at the base of the sequence suggests that at least part of this ice accumulation may have occurred only shortly prior to this main eruptive phase. Although the ring faulting associated with caldera formation is likely to be the primary control on the location of these lavas at the top of the caldera wall, there is potential evidence for the intra-caldera ice also having some influence. The columnar jointing parallel to the margins of the feeder dykes (e.g. Fig. 10c) indicates rapid cooling at the caldera wall face, suggesting that these dykes were inhibited and cooled by the ice at the surface. Hence extrusion may have been focussed near the top of the caldera wall where the ice was thin, rather than into the caldera. However, the geophysical survey of the caldera by Gilbert et al. (1996) suggests that there are lavas at the base of the caldera wall, particularly on the eastern and southern sides, which these authors inferred were erupted subglacially in association with the circum-caldera lavas; thus extrusion may not have been entirely confined to the top of the caldera margin.

4.4. Discussion

Fig. 11 summarises our preferred interpretation of part of the coupled glacial and eruptive history of Volcán Sollipulli that is recorded on its upper flanks. The absolute ice thickness under which some of the eruptions are inferred to have occurred is difficult to constrain without indicative lithofacies associations (e.g., passage zones: e.g., Skilling, 2002; Smellie, 2006) or analysis of the degassing of volatiles from glass or lava samples (Dixon et al., 2002; Tuffen et al., 2010). Even the relative ice extent is ambiguous in some cases, due to the many additional potential controls on eruption style and thus the resultant lithofacies. For example, it is not certain that the Sharkfin lava subsequence interacted with snow or ice during its emplacement, as discussed in Section 4.1.1. The local occurrence of the lava subsequence above the hyaloclastite suggests that these lavas could have been erupted under ice, but their presence beneath the hyaloclastite subsequence in all locations where its base is exposed indicates that there was a widespread shift to conditions favourable to meltwater ponding, which we consider to be most plausibly explained by glacierisation. Additionally, the ice thickness associated with Dalsheidi-type sequences, which we consider analogous to the Sharkfin debris flow subsequence, has been disputed (Smellie, 2008; Banik et al., 2014). This is discussed in Section 4.1.3, where we suggest that the field evidence is more consistent with the model of emplacement under thick ice. Palaeoclimate/glaciology studies have inferred an ice thickness (albeit poorly constrained) of ≥1 km on this part of the Andes at the LGM (e.g., Hulton et al., 2002), so the thick ice model is plausible in this case. Further study of similar sequences is necessary to better understand their formation.

The interpretation presented here differs from that of Gilbert et al. (1996) in that we infer an increase in ice thickness with time during the emplacement of the Sharkfin sequence, rather than an evolution from subglacial to subaerial eruptions. This is due to our observations (described further in Sections 3.2 and 3.4) that (1) there are lavas with features suggestive of meltwater influence at the base of the sequence, (2) the hyaloclastite subsequence is widely distributed, suggestive of emplacement under an ice cap (as opposed to in localised ponds of meltwater), (3) the debris flow subsequence has sills at its base, perhaps intruded beneath thick ice, and upper units comprising tuff-breccia rather than tephra, and (4) the subaerial lavas previously considered the top part of this sequence appear to have erupted after formation of the caldera. Conversely, we concur with the interpretation of the circum-caldera lavas in Gilbert et al. (1996). They noted that there are relatively few calderas recognised to have ring vents, and that it is rare for eruptions from these to significantly build up the caldera walls, as at Sollipulli; they also hypothesise that the intra-caldera ice may have restrained eruptions from the caldera floor. The morphological features of the lava cliffs described in Section 3.3 indicate that the intra-caldera ice was responsible for their formation. In addition, we find some evidence that the ice also could have been a contributing factor to the focussing of the vents on the caldera rim. There are a significant number of poorly studied ice-filled calderas in the southern Andes (Fig. 1) and other high-latitude continental arcs that could be investigated to assess if there is an association between ring vents and intra-caldera ice loading.

The glacial conditions at the time of the caldera-forming event are uncertain: the time period bounded by the youngest unambiguously pre-caldera (350 ± 90 ka) and oldest unequivocally post-caldera (68 ± 14 ka) Ar–Ar dates (Table 1) spans three glacial cycles. However, the predominantly subaerial Northwest lava sequence, Ar–Ar dates for which indicate an age of ~110 ka (Table 1; Jara and Moreno, in preparation), during or following the last interglacial (MIS 5e, ~123–109 ka; Lisiecki and Raymo, 2005), is thought to have been erupted after the subglacial Sharkfin sequence but prior to caldera formation (Gilbert et al., 1996). If correct, the caldera-forming event must have occurred early in the last glacial period; the extent of glaciation at this time would have been less than at the LGM, but is otherwise poorly constrained (Rabassa, 2008). There is some evidence from Kamchatka (Bindeman et al., 2010) and numerical modelling (Geyer and Bindeman, 2011) that suggested that caldera-forming large explosive eruptions are more likely during glacial periods. However, the timing of the assumed caldera-forming eruptions relative to glaciations is

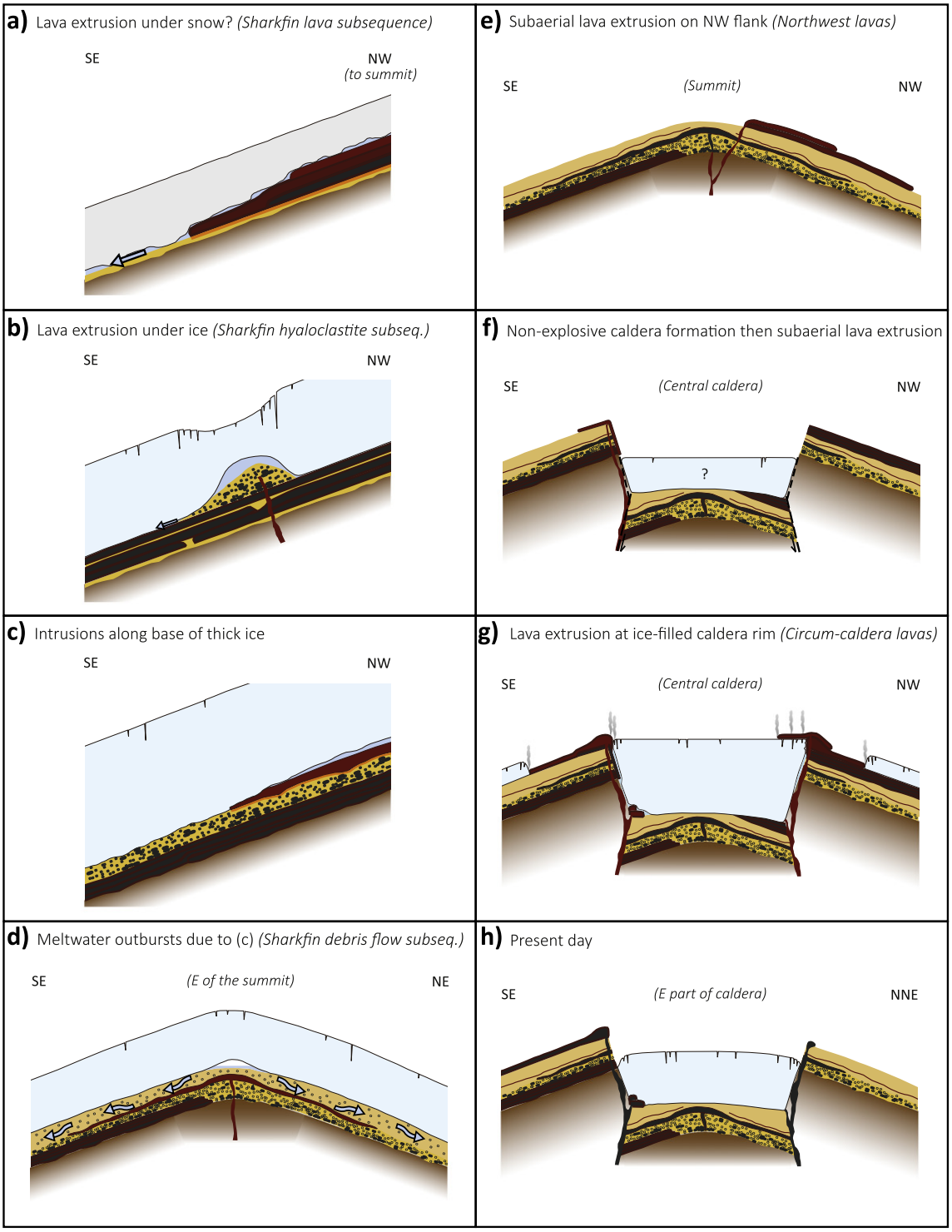

Fig. 11. Schematic illustration of part of the glacial and eruptive history of Volcán Sollipulli based upon the interpretations presented here and in Gilbert et al. (1996). Note the variations in the approximate orientation and extent of the schematic cross-sections, and that they are not to scale. (a) Emplacement of the Sharkfin lava subsequence (Section 4.1.1): summit or upper flank effusive eruption of mafic lava, which flows downslope, perhaps below thin ice or snow cover. Any meltwater generated rapidly drains away from the lava, so only the surfaces of the lavas are fragmented. Pauses in effusion are marked by deposition of thin layers of fine-grained palagonitised material, likely remobilised from hyaloclastic deposits upslope. (b) Emplacement of the Sharkfin hyaloclastite subsequence (Section 4.1.2): upper flank effusive eruption of mafic lava, generating meltwater that ponds at the source, probably due to a thick ice overburden restricting drainage. As a result, pillow lava is erupted, and tuff-breccia forms by in-situ quench fragmentation and palagonitisation of the lava; this is partly remobilised downslope, causing mechanical fragmentation. (c) Mafic lava is emplaced as sills along the interface between the bedrock and a thick ice cap, due to the ice overburden (Section 4.1.3). (d) Emplacement of the Sharkfin debris flow subsequence (Section 4.1.3): the meltwater generated by the emplacement of these sills escapes in periodic meltwater outbursts, eroding and redepositing hyaloclastic lithofacies. Sill propagation continues through the lower part of these deposits. (e) Emplacement of the subaerial Northwest lava sequence (Table 1; Gilbert et al., 1996) after melting of the ice cap. (f) Formation of the caldera by a non-explosive mechanism, followed by emplacement of subaerial lavas of intermediate composition on parts of the top of the caldera wall (Section 3.3). (g) Emplacement of the bulk of the circum-caldera lava sequence (Section 4.3): after the caldera has filled with ice, further effusive eruption of intermediate-composition lava occurs around the caldera wall (fed from dykes along the ring fault). Domes on and flows from the top of the caldera wall are buttressed by the intra-caldera ice, but become subaerial above the ice level. Some lava extrusion at the base of the caldera rim is suggested by geophysical data (Gilbert et al., 1996). (h) A schematic section through the caldera at the present day. This follows the Alpehué and Chufquén eruptions and ice advance and retreat into/from the Chufquén valley and Alpehué crater (all not shown), which are described by Gilbert et al. (1996).

poorly constrained for the majority of those events studied by Bindeman et al. (2010). Although tephra is less likely to be preserved when deposited supraglacially (Hobbs, 2014), the subsequent glacial advance (leading up to the LGM) alone would be sufficient to account for the absence of evidence for an explosive origin of the caldera, considering that no tephras deposited prior to local deglaciation have been found in the region (Fontijn et al., 2014). Nevertheless, the ~60 m maximum subsidence of the Bárðarbunga caldera in Iceland associated with the 2014–15 Holuhraun eruption (Riel et al., 2015; Sigmundsson et al., 2015) highlights the potential for subglacial caldera formation without an explosive eruption. Additional dating of eruptive sequences is critical to better constrain the climate at the time (and thus to inform speculation about the mechanism) of formation of the caldera at Sollipulli.

As outlined in Section 1, most glaciovolcanism described at other arc stratovolcanoes at temperate latitudes comprises coherent lavas, similar to the Chufquén valley lavas and circum-caldera lava sequence. Nevertheless, the Sharkfin sequence indicates that it is possible, although perhaps difficult, for extensive (i.e., not topographically confined) fragmental lithofacies to be produced by subglacial eruptions on such volcanoes. It is unclear why these lithofacies are relatively uncommon, including elsewhere in the Andean Southern Volcanic Zone (SVZ) (although hyaloclastite has been reported locally at Nevados de Chillán and more widely at Volcán Hudson: Gutiérrez et al., 2005; Mee et al., 2006). It is not necessarily because the magma is typically of an evolved composition, as there are examples in Iceland of fragmental deposits from subglacial eruptions of intermediate magmas (e.g., Stevenson et al., 2009) and rhyolite (e.g., McGarvie et al., 2007), although often they are only associated with mafic eruptions (e.g., Kelman et al., 2002). In any case, mafic volcanism is thought to be predominant in the central and southern sectors of the SVZ (Stern, 2004; Fontijn et al., 2014). There could be preservation bias; fragmental lithofacies are more easily eroded than lavas, and they could have been covered by the large volume of post-glacial lavas thought to have been erupted at some volcanoes (e.g., Llaima and Villarrica: Naranjo and Moreno, 1991). Alternatively, their absence could suggest a reduction in the frequency and/or volume of eruptions during glacial maxima, for which there is some evidence in the record of explosive eruptions (Watt et al., 2013; Rawson et al., 2015). Further detailed mapping of the volcanoes of the SVZ and in similar arcs is essential to quantify the prevalence of subglacial eruptions at such volcanoes.

5. Conclusions

The glaciovolcanic eruption products preserved at Volcán Sollipulli provide new insight into the range of volcano–ice interactions that can occur on ice-capped stratovolcanoes. Widespread hyaloclastic tuff-breccia, sometimes containing lava pillows, suggests that considerable lava–meltwater interaction can occur beneath ice on such edifices apparently without topographic confinement. Furthermore, an extensive sequence of sills and debris flow deposits is recognised for the first time on a temperate-latitude stratovolcano, which, considering its similarity to Dalsheidi-type sequences, also suggests ubiquitous syn-eruptive subglacial meltwater generation and ponding. Nevertheless, the ice thickness during the emplacement of these units is not possible to constrain robustly from the lithofacies relationships. The lavas emplaced around the caldera rim and on the upper flanks exemplify the variety of interactions (and morphologies resulting from) lava flowing beneath or into ice, including that platy fracturing of the lava margin can occur, which has not been widely recognised in such lavas. Features of the circum-caldera lava sequence constrain the thickness of the intra-caldera ice during its emplacement, and also suggest that the ice might have considerably influenced the evolution of the caldera itself. Constraining the prevalence and nature of subglacial and other glaciovolcanic activity at similar volcanoes will be essential to further understanding of the influence of ice on arc volcanism.

Acknowledgements

This work was supported by the International Association of Volcanology and Chemistry of the Earth's Interior project 'Ice-filled calderas in the 21st Century: consequences of volcanic unrest and environmental change', Natural Environment Research Council (NERC) project 'Tempo of post-glacial volcanism in southern Chile' (NE/I013210/1), and studentships to S.M. Lachowycz from the NERC (NE/I528485/1), British Geological Survey University Funding Initiative (S198), and University College Oxford. D.M. Pyle and T.A. Mather are supported by and contribute to the NERC Centre for the Observation and Modelling of Earthquakes, Volcanoes and Tectonics (COMET). J.A. Naranjo acknowledges funding from FONDECYT (project 1960186). L.K. Hobbs was supported by a Lancaster University studentship and funding from the British Geological Survey. We thank Neil Slatcher (Lancaster University), Oscar Bustamente (Universidad de Chile), and Ñuke Mapu guides for fieldwork assistance, as well as M. Mangan for editorial handling and J.L. Smellie and an anonymous reviewer for reviews that greatly improved this article.

Appendix A. Supplementary data

Supplementary data to this article can be found online at http://dx.doi.org/10.1016/j.scitotenv.2015.06.149.

References

Arancibia, G., Matthews, S.J., Perez de Arce, C., 2006. K–Ar and $^{40}Ar/^{39}Ar$ geochronology of supergene processes in the Atacama Desert, Northern Chile: tectonic and climatic relations. J. Geol. Soc. Lond. 163, 107–118. http://dx.doi.org/10.1144/0016-764904-161.

Banik, T.J., Wallace, P.J., Höskuldsson, Á., Miller, C.F., Bacon, C.R., Furbish, D.J., 2014. Magma–ice–sediment interactions and the origin of lava/hyaloclastite sequences in the Síða formation, South Iceland. Bull. Volcanol. 76, 785. http://dx.doi.org/10.1007/s00445-013-0785-3.

Belousov, A., Behncke, B., Belousova, M., 2011. Generation of pyroclastic flows by explosive interaction of lava flows with ice/water-saturated substrate. J. Volcanol. Geotherm. Res. 202, 60–72. http://dx.doi.org/10.1016/j.jvolgeores.2011.01.004.

Bindeman, I.N., Leonov, V.L., Izbekov, P.E., Ponomareva, V.V., Watts, K.E., Shipley, N.K., Perepelov, A.B., Bazanova, L.I., Jicha, B.R., Singer, B.S., Schmitt, A.K., Portnyagin, M.V., Chen, C.H., 2010. Large-volume silicic volcanism in Kamchatka: Ar–Ar and U–Pb ages, isotopic, and geochemical characteristics of major pre-Holocene caldera-forming eruptions. J. Volcanol. Geotherm. Res. 189, 57–80. http://dx.doi.org/10.1016/j.jvolgeores.2009.10.009.

Bird, P., 2003. An updated digital model of plate boundaries. Geochem. Geophys. Geosyst. 4, 1027–1079. http://dx.doi.org/10.1029/2001GC000252.

Björnsson, H., 2002. Subglacial lakes and jökulhlaups in Iceland. Glob. Planet. Chang. 25, 255–271. http://dx.doi.org/10.1016/S0921-8181(02)00130-3.

Bonnichsen, B., Kauffmann, D.F., 1987. Physical features of rhyolite lava flows in the Snake River Plain volcanic province, southwestern Idaho. In: Fink, J.H. (Ed.), The Emplacement of Silicic Domes and Lava FlowsSpec. Pap. Geol. Soc. Am. 212. Geological Society of America, pp. 119–145. http://dx.doi.org/10.1130/SPE212-p119.

Bronk Ramsey, C., 2009. Bayesian analysis of radiocarbon dates. Radiocarbon 51, 337–360. http://dx.doi.org/10.2458/azu_js_rc.v.3494.

Clark, P.U., Dyke, A.S., Shakun, J.D., Carlson, A.E., Clark, J., Wohlfarth, B., Mitrovica, J.X., Hostetler, S.W., McCabe, A.M., 2009. The Last Glacial Maximum. Science 325, 710–714. http://dx.doi.org/10.1126/science.1172873.

Conway, C.E., Townsend, D.B., Leonard, G.S., Wilson, C.J.N., Calvert, A.T., Gamble, J.A., 2015. Lava–ice interaction on a large composite volcano: a case study from Ruapehu, New Zealand. Bull. Volcanol. 77, 21. http://dx.doi.org/10.1007/s00445-015-0906-2.

De Vleeschouwer, F., 2002. Etude tephrostratigraphique de depôts Holocènes des bassins versants de deux lacs Chiliens — Exemple del lacs Icalma et Galletue (Chili — 38°S, 71°W) Thesis, Université de Liège, Belgium.

DeGraff, J.M., Aydin, A., 1987. Surface morphology of columnar joints and its significance to mechanics and direction of joint growth. Geol. Soc. Am. Bull. 99, 605–617. http://dx.doi.org/10.1130/0016-7606(1987)99<605:SMOCJA>2.0.CO;2.

Dixon, J.E., Filiberto, J.R., Moore, J.G., Hickson, C.J., 2002. Volatiles in basaltic glasses from a subglacial volcano in northern British Columbia (Canada): implications for ice sheet thickness and mantle volatiles. In: Smellie, J.L., Chapman, M.G. (Eds.), Volcano–Ice Interactions on Earth and Mars, Geol. Soc. Spec. Publ. 202. Geological Society, London, pp. 255–271. http://dx.doi.org/10.1144/GSL.SP.2002.202.01.13.

Edwards, B.R., Russell, J.K., 2002. Glacial influences on morphology and eruptive products of Hoodoo Mountain volcano, Canada. In: Smellie, J.L., Chapman, M.G. (Eds.), Volcano–ice interactions on Earth and MarsGeol. Soc. Spec. Publ. 202. Geological Society, London, pp. 179–194. http://dx.doi.org/10.1144/GSL.SP.2002.202.01.09.

Edwards, B.R., Russell, J.K., 2011. Thermodynamic constraints on explosive vs. effusive onset of glaciovolcanic eruptions. American Geophysical Union Fall Meeting 2011 (Abstract #V31E-2578).

Fisher, R.V., Schmincke, H.-U., 1984. Alteration of volcanic glass. In: Fisher, R.V., Schmincke, H.-U. (Eds.), Pyroclastic Rocks. Springer, New York, pp. 312–345.

Fontijn, K., Lachowycz, S.M., Rawson, H., Pyle, D.M., Mather, T.A., Naranjo, J.A., Moreno-Roa, H., 2014. Late Quaternary tephrostratigraphy of southern Chile and Argentina. Quat. Sci. Rev. 89, 70–84. http://dx.doi.org/10.1016/j.quascirev.2014.02.007.

Fontijn, K., Rawson, H., Van Daele, M., Moernaut, J., Abarzúa, A.M., Heirman, K., Bertrand, S., Pyle, D.M., Mather, T.A., De Batist, M., Naranjo, J.A., Moreno, H., 2015. Synchronisation of sedimentary records using tephra: A post-glacial tephrochronological model for the Chilean Lake District (in preparation).

Forbes, A.E.S., Blake, S., McGarvie, D.W., Tuffen, H., 2012. Pseudopillow fracture systems in lavas: insights into cooling mechanisms and environments from lava flow fractures. J. Volcanol. Geotherm. Res. 245–246, 68–80. http://dx.doi.org/10.1016/j.jvolgeores.2012.07.007.

Forbes, A.E.S., Blake, S., Tuffen, H., 2014a. Entablature: fracture types and mechanisms. Bull. Volcanol. 76, 820–833. http://dx.doi.org/10.1007/s00445-014-0820-z.

Forbes, A.E.S., Blake, S., Tuffen, H., Wilson, A., 2014b. Fractures in a trachyandesitic lava at Öræfajökull, Iceland, used to infer subglacial emplacement in 1727–8 eruption. J. Volcanol. Geotherm. Res. 288, 8–18. http://dx.doi.org/10.1016/j.jvolgeores.2014.10.004.

Geyer, A., Bindeman, I., 2011. Glacial influence on caldera-forming eruptions. J. Volcanol. Geotherm. Res. 202, 127–142. http://dx.doi.org/10.1016/j.jvolgeores.2011.02.001.

Gilbert, J.S., Stasiuk, M.V., Lane, S.J., Adam, C.R., Murphy, M.D., Sparks, R.S.J., Naranjo, J.A., 1996. Non-explosive, constructional evolution of the ice-filled caldera at Volcán Sollipulli, Chile. Bull. Volcanol. 58, 67–83. http://dx.doi.org/10.1007/s004450050127.

Glasser, N.F., Jansson, K.N., Harrison, S., Kleman, J., 2008. The glacial geomorphology and Pleistocene history of South America between 38°S and 56°S. Quat. Sci. Rev. 27, 365–390. http://dx.doi.org/10.1016/j.quascirev.2007.11.011.

Goehring, L., Morris, S.W., 2008. Scaling of columnar joints in basalt. J. Geophys. Res. 113, B10203. http://dx.doi.org/10.1029/2007JB005018.

Gutiérrez, F., Gioncada, A., González Ferran, O., Lahsen, A., Mazzuoli, R., 2005. The Hudson Volcano and surrounding monogenetic centres (Chilean Patagonia): an example of volcanism associated with ridge–trench collision environment. J. Volcanol. Geotherm. Res. 145, 207–233. http://dx.doi.org/10.1016/j.jvolgeores.2005.01.014.

Hobbs, L.K., 2014. The Role of Cold Supraglacial Volcanic Deposits in Influencing Glacial Ablation PhD thesis, Lancaster University, United Kingdom.

Hogg, A.G., Hua, Q., Blackwell, P.G., Niu, M., Buck, C.E., Guilderson, T.P., Heaton, T.J., Palmer, J.G., Reimer, P.J., Reimer, R.W., Turney, C.S.M., Zimmerman, S.R.H., 2013. SHCal13 Southern Hemisphere calibration, 0–50,000 years cal BP. Radiocarbon 55, 1889–1903. http://dx.doi.org/10.2458/azu_js_rc.55.16783.

Höskuldsson, A., Sparks, R.S.J., 1997. Thermodynamics and fluid dynamics of effusive subglacial eruptions. Bull. Volcanol. 59, 219–230. http://dx.doi.org/10.1007/s004450050187.

Huggel, C., 2009. Recent extreme slope failures in glacial environments: effects of thermal perturbation. Quat. Sci. Rev. 28, 1119–1130. http://dx.doi.org/10.1016/j.quascirev.2008.06.007.

Hulton, N.R.J., Purves, R.S., McCulloch, R.D., Sugden, D.E., Bentley, M.J., 2002. The Last Glacial Maximum and deglaciation in southern South America. Quat. Sci. Rev. 21, 233–241. http://dx.doi.org/10.1016/S0277-3791(01)00103-2.

Jara, C., Moreno, H., 2015. Geología del Volcán Sollipulli, Región de la Araucanía. Carta Geológica de Chile, Servicio Nacional de Geología y Minería (in preparation).

Kelman, M.C., Russell, J.K., Hickson, C.J., 2002. Effusive intermediate volcanism in the Garibaldi Volcanic Belt, southwestern British Columbia, Canada. In: Smellie, J.L., Chapman, M.G. (Eds.), Volcano–Ice Interactions on Earth and Mars, Geol. Soc. Spec. Publ. 202. Geological Society, London, pp. 195–211. http://dx.doi.org/10.1144/GSL.SP.2002.202.01.10.

Le Bas, M.J., Le Maitre, R.W., Streckeisen, A., Zanettin, B., 1985. A chemical classification of volcanic rocks based on the total alkali–silica diagram. J. Petrol. 27, 745–750.

Lescinsky, D.T., Fink, J.H., 2000. Lava and ice interaction at stratovolcanoes: use of characteristic features to determine past glacial extents and future volcanic hazards. J. Geophys. Res. 105, 23711–23726. http://dx.doi.org/10.1029/2000JB900214.

Lescinsky, D.T., Sisson, T.W., 1998. Ridge-forming, ice-bounded lava flows at Mount Rainier, Washington. Geology 26, 351–354. http://dx.doi.org/10.1130/0091-7613(1998)026<0351:RFIBLF>2.3.CO;2.

Lisiecki, L.E., Raymo, M.E., 2005. A Pliocene–Pleistocene stack of 57 globally distributed benthic $\delta^{18}O$ records. Paleoceanography 20, PA1003. http://dx.doi.org/10.1029/2004PA001071.

Lodge, R.W.D., Lescinsky, D.T., 2009. Fracture patterns at lava–ice contacts on Kokostick Butte, OR, and Mazama Ridge, Mount Rainier, WA: implications for flow emplacement and cooling histories. J. Volcanol. Geotherm. Res. 185, 298–310. http://dx.doi.org/10.1016/j.jvolgeores.2008.10.010.

Long, P.E., Wood, B.J., 1986. Structures, textures, and cooling histories of Columbia River basalt flows. Geol. Soc. Am. Bull. 97, 1144–1155. http://dx.doi.org/10.1130/0016-7606(1986)97<1144:STACHO>2.0.CO;2.

López-Escobar, L., Cembrano, J., Moreno, H., 1995. Geochemistry and tectonics of the Chilean Southern Andes basaltic Quaternary volcanism (37–46°S). Rev. Geol. Chile 22, 219–234. http://dx.doi.org/10.5027/andgeoV22n2-a06.

Loughlin, S.C., 2002. Facies analysis of proximal subglacial and proglacial volcaniclastic successions at the Eyjafjallajökull central volcano, southern Iceland. In: Smellie, J.L., Chapman, M.G. (Eds.), Volcano–Ice Interactions on Earth and Mars, Geol. Soc. Spec. Publ. 202. Geological Society, London, pp. 149–178.

Major, J.J., Newhall, C.G., 1989. Snow and ice perturbation during historical volcanic eruptions and the formation of lahars and floods: a global review. Bull. Volcanol. 52, 1–27. http://dx.doi.org/10.1007/BF00641384.

Matthews, K.J., Muller, R.D., Wessel, P., Whittaker, J.M., 2011. The tectonic fabric of the ocean basins. J. Geophys. Res. 116, B12109. http://dx.doi.org/10.1029/2011JB008413.

McGarvie, D.W., Stevenson, J.A., Burgess, R., Tuffen, H., Tindle, A.G., 2007. Volcano–ice interactions at Prestahnúkur, Iceland: rhyolite eruption during the last interglacial–glacial transition. Ann. Glaciol. 45, 38–47. http://dx.doi.org/10.3189/172756407782282453.

Mee, K., Tuffen, H., Gilbert, J.S., 2006. Snow-contact volcanic facies and their use in determining past eruptive environments at Nevados de Chillán volcano, Chile. Bull. Volcanol. 68, 363–376. http://dx.doi.org/10.1007/s00445-005-0017-6.

Mee, K., Gilbert, J.S., McGarvie, D.W., Naranjo, J.A., Pringle, M.S., 2009. Palaeoenvironment reconstruction, volcanic evolution and geochronology of the Cerro Blanco subcomplex, Nevados de Chillán volcanic complex, central Chile. Bull. Volcanol. 71, 933–952. http://dx.doi.org/10.1007/s00445-009-0277-7.

Murphy, M.D., 1996. Magmatic Evolution at Volcán Sollipulli, Southern Andes of Chile PhD thesis University of Bristol, United Kingdom.

Naranjo, J.A., Moreno, H., 1991. Actividad explosive postglacial en el Volcan Llaima, Andes del Sur (38°45′S). Rev. Geol. Chile 18, 69–80. http://dx.doi.org/10.5027/andgeoV18n1-a06.

Naranjo, J.A., Moreno, H., Banks, N.G., 1993a. La erupción del Volcán Hudson en 1991 (46°S), Región XI, Aisén, Chile. Serv. Nac. Geol. Min. Bol. 44, 1–50.

Naranjo, J.A., Moreno, H., Emparan, C., Murphy, M.D., 1993b. Volcanismo explosivo reciente en la caldera del volcán Sollipulli, Andes del Sur (39°S). Rev. Geol. Chile 20, 167–191. http://dx.doi.org/10.5027/andgeoV20n2-a03.

Pollock, M., Edwards, B., Hauksdóttir, S., Alcorn, R., Bowman, L., 2014. Geochemical and lithostratigraphic constraints on the formation of pillow-dominated tindars from Undirhlíðar quarry, Reykjanes Peninsula, Southwest Iceland. Lithos 200–201, 317–333. http://dx.doi.org/10.1016/j.lithos.2014.04.023.

Porębski, S.J., Gradziński, R., 1990. Lava-fed Gilbert-type delta in the Polonez Cove Formation (Lower Oligocene), King George Island, West Antarctica. In: Colella, A., Prior, D.B. (Eds.), Coarse-Grained Deltas, 10.1002/9781444303858.ch19. Spec. Pub. Int. Ass. Sediment. 10, pp. 335–351.

Rabassa, J., 2008. Late Cenozoic glaciations in Patagonia and Tierra del Fuego. In: Rabassa, J. (Ed.), The Late Cenozoic of Patagonia and Tierra del FuegoDevelopments in Quaternary Science 11. Elsevier, pp. 151–204. http://dx.doi.org/10.1016/S1571-0866(07)10008-7.

Ramsey, M.H., Potts, P.J., Webb, P.C., Watkins, P., Watson, J.S., Coles, B.J., 1995. An objective assessment of analytical method precision: comparison of ICP-AES and XRF for the analysis of silicate rocks. Chem. Geol. 124, 1–19. http://dx.doi.org/10.1016/0009-2541(95)00020-M.

Rawson, H., Naranjo, J.A., Smith, V.C., Fontijn, K., Pyle, D.M., Mather, T.A., Moreno, H., 2015. The frequency and magnitude of post-glacial explosive eruptions at Volcán Mocho-Choshuenco, southern Chile. J. Volcanol. Geotherm. Res. 299, 103–129. http://dx.doi.org/10.1016/j.jvolgeores.2015.04.003.

Riel, B., Milillo, P., Simons, M., Lundgren, P., Kanamori, H., Samsonov, S., 2015. The collapse of Bárðarbunga caldera, Iceland. Geophys. J. Int. 202, 446–453. http://dx.doi.org/10.1093/gji/ggv157.

Rittman, A., 1958. Il meccanismo di formazione delle lave a pillows e dei cosidelti tufi palagonitici. Att. Acad. Gioenia 4, 310–317.

Rivera, A., Bown, F., 2013. Recent glacier variations on active ice capped volcanoes in the Southern Volcanic Zone (37–46°S), Chilean Andes. J. S. Am. Earth Sci. 45, 345–356. http://dx.doi.org/10.1016/j.jsames.2013.02.004.

Russell, J.K., Edwards, B.R., Porritt, L., Ryane, C., 2014. Tuyas: a descriptive genetic classification. Quat. Sci. Rev. 87, 70–81. http://dx.doi.org/10.1016/j.quascirev.2014.01.001.

Schaefer, J.M., Putnam, A.E., Denton, G.H., Kaplan, M.R., Birkel, S., Doughty, A.M., Kelley, S., Barrell, D.J.A., Finkel, R.C., Winckler, G., Anderson, R.F., Ninneman, U.S., Barker, S., Schwartz, R., Andersen, B.J., Schluechter, C., 2015. The Southern Glacial Maximum 65,000 years ago and its unfinished termination. Quat. Sci. Rev. 114, 52–60. http://dx.doi.org/10.1016/j.quascirev.2015.02.009.

Schmidt, M.E., Grunder, A.L., 2009. The evolution of North Sister: a volcano shaped by extension and ice in the central Oregon Cascade. Arc. Geol. Soc. Am. Bull. 121, 643–662. http://dx.doi.org/10.1016/10.1130/B26442.1.

Schopka, H.H., Gudmundsson, M.T., Tuffen, H., 2006. The formation of Helgafell, southwest Iceland, a monogenetic subglacial hyaloclastite ridge: sedimentology, hydrology and volcano–ice interaction. J. Volcanol. Geotherm. Res. 152, 359–377. http://dx.doi.org/10.1016/j.jvolgeores.2005.11.010.

Siebert, L., Simkin, T., Kimberly, P., 2010. Volcanoes of the World. Third edition. University of California Press, Berkeley.

Sigmundsson, F., Hooper, A., Hreinsdóttir, S., Vogfjörd, K.S., Ófeigsson, B.G., Heimisson, E.R., Dumont, S., Parks, M., Spaans, K., Gudmundsson, G.B., Drouin, V., Árnadóttir, T., Jónsdóttir, K., Gudmundsson, M.T., Högnadóttir, T., Fridriksdóttir, H.M., Hensch, M., Einarsson, P., Magnússon, E., Samsonov, S., Brandsdóttir, B., White, R.S., Ágústsdóttir, T., Greenfield, T., Green, R.G., Hjartardóttir, A.R., Pedersen, R., Bennett, R.A., Geirsson, H., La Femina, P.C., Björnsson, H., Pálsson, F., Sturkell, E., Bean, C.J., Möllhoff, M., Braiden, A.K., Eibl, E.P.S., 2015. Segmented lateral dyke growth in a rifting event at Bárðarbunga volcanic system, Iceland. Nature 517, 191–195. http://dx.doi.org/10.1038/nature14111.

Skilling, I., 2002. Basaltic pahoehoe lava-fed deltas: large-scale characteristics, clast generation, emplacement processes and environmental discrimination. In: Smellie, J.L., Chapman, M.G. (Eds.), Volcano–Ice Interactions on Earth and MarsGeol. Soc. Spec. Publ. 202. Geological Society, London, pp. 91–113. http://dx.doi.org/10.1144/GSL.SP.2002.202.01.06.

Skilling, I., 2009. Subglacial to emergent basaltic volcanism at Hlöðufell, south-west Iceland: a history of ice-confinement. J. Volcanol. Geotherm. Res. 185, 276–289. http://dx.doi.org/10.1016/j.jvolgeores.2009.05.023.

Smellie, J.L., 2006. The relative importance of supraglacial versus subglacial meltwater escape in basaltic subglacial tuya eruptions: an important unresolved conundrum. Earth-Sci. Rev. 74, 241–268. http://dx.doi.org/10.1016/j.earscirev.2005.09.004.

Smellie, J.L., 2008. Basaltic subglacial sheet-like sequences: evidence for two types with different implications for the inferred thickness of associated ice. Earth-Sci. Rev. 88, 60–88. http://dx.doi.org/10.1016/j.earscirev.2008.01.004.

Smellie, J.L., 2009. Terrestrial sub-ice volcanism: landform morphology, sequence characteristics, environmental influences, and implications for candidate Mars examples. In:

Chapman, M.G., Keszthelyi, L.P. (Eds.), Preservation of Random Megascale Events on Mars and Earth: Influence on Geologic History. Geological Society of America Special Paper 453, pp. 55–76. http://dx.doi.org/10.1130/2009.453(05).

Smellie, J.L., 2013. Quaternary vulcanism: subglacial landforms. In: Elias, S.A. (Ed.), Encyclopedia of Quaternary Science, second edition, pp. 780–802 http://dx.doi.org/10.1016/B978-0-444-53643-3.00074-1.

Smellie, J.L., Chapman, M.G., 2002. Volcano–ice interaction on Earth and Mars. Geol. Soc. Lond. Spec. Publ. 202.

Smellie, J.L., Skilling, I.P., 1994. Products of subglacial volcanic eruptions under different ice thicknesses: two examples from Antarctica. Sediment. Geol. 91, 115–129. http://dx.doi.org/10.1016/0037-0738(94)90125-2.

Smellie, J.L., Hole, M.J., Nell, P.A.R., 1993. Late Miocene valley-confined subglacial volcanism in northern Alexander Island, Antarctic Peninsula. Bull. Volcanol. 55, 273–288. http://dx.doi.org/10.1007/BF00624355.

Smellie, J.L., Rocchi, S., Gemelli, M., Di Vincenzo, G., Armienti, P., 2011. A thin predominantly cold-based Late Miocene East Antarctic ice sheet inferred from glaciovolcanic sequences in northern Victoria Land, Antarctica. Palaeogeogr. Palaeoclimatol. Palaeoecol. 307, 129–149. http://dx.doi.org/10.1016/j.palaeo.2011.05.008.

Smellie, J.L., Wilch, T.I., Rocchi, S., 2013. 'A'ā lava-fed deltas: a new reference tool in paleoenvironmental studies. Geology 41, 403–406. http://dx.doi.org/10.1130/G33631.1.

Smellie, J.L., Rocchi, S., Wilch, T.I., Gemelli, M., Di Vincenzo, G., McIntosh, W., Dunbar, N., Panter, K., Fargo, A., 2014. Glaciovolcanic evidence for a polythermal Neogene East Antarctic Ice Sheet. Geology 42, 39–41. http://dx.doi.org/10.1130/G34787.1.

Spörli, K.B., Rowland, J.V., 2006. 'Column on column' structures as indicators of lava/ice interaction, Ruapehu andesite volcano, New Zealand. J. Volcanol. Geotherm. Res. 157, 294–310. http://dx.doi.org/10.1016/j.jvolgeores.2006.04.004.

Stern, C.R., 2004. Active Andean volcanism: its geologic and tectonic setting. Rev. Geol. Chile 31, 161–206. http://dx.doi.org/10.4067/S0716-02082004000200001.

Stevenson, J.A., Smellie, J.L., McGarvie, D.W., Gilbert, J.S., Cameron, B.I., 2009. Subglacial intermediate volcanism at Kerlingarfjöll, Iceland: magma–water interactions beneath thick ice. J. Volcanol. Geotherm. Res. 185, 337–351. http://dx.doi.org/10.1016/j.jvolgeores.2008.12.016.

Tuffen, H., 2007. Models of ice melting and edifice growth at the onset of subglacial basaltic eruptions. J. Geophys. Res. 112, B03203. http://dx.doi.org/10.1029/2006JB004523.

Tuffen, H., 2010. How will melting of ice affect volcanic hazards in the twenty-first century? Philos. Trans. R. Soc. Lond. A 368, 2535–2558. http://dx.doi.org/10.1098/rsta.2010.0063.

Tuffen, H., Owen, J., Denton, J., 2010. Magma degassing during subglacial eruptions and its use to reconstruct palaeo-ice thicknesses. Earth-Sci. Rev. 99, 1–18. http://dx.doi.org/10.1016/j.earscirev.2010.01.001.

Tuffen, H., James, M.R., Castro, J.M., Schipper, C.I., 2013. Exceptional mobility of an advancing rhyolitic obsidian flow at Cordón Caulle volcano in Chile. Nat. Commun. 4, 2709. http://dx.doi.org/10.1038/ncomms3709.

USGS and Japan ASTER program, 2012. ASTER scene AST_14DMO_003_02182005144538.3. USGS, Sioux Falls (18 February 2005).

Watt, S.F.L., Pyle, D.M., Mather, T.A., 2013. The volcanic response to glaciation: evidence from glaciated arcs and a reassessment of global eruption records. Earth-Sci. Rev. 122, 77–102. http://dx.doi.org/10.1016/j.earscirev.2013.03.007.

Watton, T.J., Jerram, D.A., Thordarson, T., Davies, R.J., 2013. Three-dimensional lithofacies variations in hyaloclastite deposits. J. Volcanol. Geotherm. Res. 250, 19–33. http://dx.doi.org/10.1016/j.jvolgeores.2012.10.011.

White, J.D.L., Houghton, B.F., 2006. Primary volcaniclastic rocks. Geology 34 (8), 677–680. http://dx.doi.org/10.1130/G22346.1.